

**THEORY OF OPTICAL CROSS SECTIONS OF DEEP LEVEL IMPURITIES IN  
COVALENTLY BONDED SEMICONDUCTORS**

by

LOWELL RICKS HAUENSTEIN, B.S. in I.E.

A THESIS

IN

PHYSICS

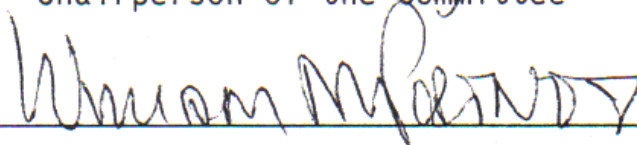
Submitted to the Graduate Faculty  
of Texas Tech University in  
Partial Fulfillment of  
the Requirements for  
the Degree of

MASTER OF SCIENCE

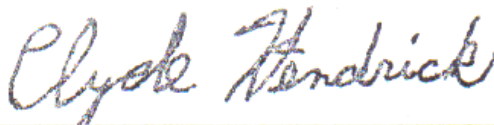
Approved



Chairperson of the Committee



Accepted



Dean of the Graduate School

May, 1988 (Revised May, 2010)

## **ACKNOWLEDGEMENTS**

For their special help in making this thesis possible, I owe grateful acknowledgement to:

Dr. Charles Myles, Professor of Physics, Texas Tech University, for his direction and patience on this research project.

The Engineering Services Department at Tracer Aerospace, Inc. for allowing me the use of their equipment during the preparation of this thesis.

And I especially want to thank Robert Gatliff, systems analyst at Tracor Aerospace, Inc. who assisted in the final printing of the graphs on the laser printer.

## TABLE OF CONTENTS

ACKNOWLEDGEMENTS .....	i i
ABSTRACT .....	v
LIST OF FIGURES .....	vi
I. INTRODUCTION .....	1
II. BACKGROUND .....	10
2.1 Hydrogenic Model For Shallow Levels ....	10
2.2 Vogl's Tight Binding Theory For Host Bandstructures .....	13
2.3 Hjalmarson's Deep Level Theory .....	14
2.4 Lucovsky's Model For Optical Cross Sections of Deep Levels .....	15
III. FORMALISM FOR THE OPTICAL CROSS SECTION .....	19
3.1 Derivation of the General Form .....	19
3.2 Form of the Cross Section in Deep Level Theory .....	23
IV. RESULTS AND CHEMICAL TRENDS .....	31
4.1 Introduction .....	31
4.2 Comparison to Lucovsky's Model .....	31
4.3 Zincblende and Diamond Lattices .....	33
4.4 Comparison of Direct Gap and Indirect Gap Materials .....	36
4.4.1. Direct Gap Materials .....	36
4.4.2. Indirect Gap Materials .....	37
4.5 Variation in Cross Sections as the Symmetry is Varied .....	39

	V. CONCLUSIONS .....	61
BIBLIOGRAPHY	.....	63
APPENDICES		
	A. NUMERICAL ANALYSIS OF THE OPTICAL CROSS SECTION .....	68
	B. OPTICAL CROSS SECTION PROGRAM LISTING .....	72

## ABSTRACT

A formalism for the calculation of the optical cross section of a deep impurity level in a covalently bonded semiconductor is developed. This formalism, which is based upon quantum mechanical time dependent perturbation theory, assumes a tight binding representation for the bandstructure of the host semiconductor and models the deep level and its associated potential using the Hjalmarson theory of deep levels. The optical cross sections for the deep levels associated with several impurities in selected semiconductors are calculated numerically using a semi-empirical tight binding bandstructure model as input into the formalism. The chemical trends which emerge from these calculations are discussed.

## LIST OF FIGURES

1.1	Energy Levels .....	6
1.2	Optical Cross Section of a Typical Semiconductor .....	8
2.1	Lucovsky's Model For Optical Cross Sections of Deep Levels, Conduction Band Only .....	17
4.1	Lucovsky's Model: Optical Cross Section For Deep Level Impurities in Si, Conduction Band Only .....	41
4.2	Optical Cross Sections For Deep Levels of A1 Symmetry in Si With Substitutional Impurities .....	43
4.3	Optical Cross Sections For Deep Levels of A1 Symmetry in Ge With Substitutional Impurities .....	45
4.4	Optical Cross Sections For Deep Levels of A1 Symmetry in GaAs With The Impurity At The As (anion) Site .....	47
4.5	Optical Cross Sections For Deep Levels of A1 Symmetry in GaP With The Impurity At The P (anion) Site .....	49
4.6	Optical Cross Sections For Deep Levels of A1 Symmetry in AlP With The Impurity At The P (anion) Site .....	51
4.7	Optical Cross Sections For Deep Levels of T2 Symmetry in GaAs With The Impurity At The Ga (cation) Site .....	53
4.8	Optical Cross Sections For Deep Levels of T2 Symmetry in ZnTe With The Impurity At The Zn (cation) Site .....	55
4.9	Optical Cross Sections For Deep Levels of T2 Symmetry in GaP With The Impurity At The Ga (cation) Site .....	57
4.10	Optical Cross Sections For Deep Levels of T2 Symmetry in AlP With The Impurity At The A1 (cation) Site .....	59

## **CHAPTER I**

### **INTRODUCTION**

Many of a semiconductor's useful electronic properties are traceable to the presence of impurities in the material. Of particular interest in this thesis are those impurities which produce energy levels near the center of the fundamental bandgap—the so-called deep level impurities that enable the semiconductor to be used in device applications, such as switching and laser applications. Although controlling such impurities is of primary concern during semiconductor device processing, the impurities must first be located and identified.

Understanding the properties of deep levels is important because controlling them will help to control the lifetime of carriers, since they act as recombination centers for the charge carriers (1, 2). The most efficient recombination takes place at levels near the middle of the bandgap. In that case, the corresponding cross section becomes very large and the carrier lifetime of the free carriers becomes very small. If large carrier lifetimes are required, deep level impurities must be avoided. One device application of deep level impurities is to light emitting diodes, which owe their existence to these defects (3). The deep levels associated with particular impurities determine the wavelength of the emitted light. However, unwanted impurities can be the limiting factor for the device due to non-radiative recombination enhancement (2, 4).

As a consequence of their importance, substantial theoretical efforts have been made to understand and predict the energies of deep level defects. All of these theories, as well as a number of experimental techniques, have increased our understanding of such defects.

One means of observing a deep energy level in a semiconductor is through optical measurements. In order to understand such measurements, the optical cross sections of the deep levels must be understood.

This thesis develops a formalism for calculating this cross section and numerically studies the chemical trends in this quantity for several deep level impurities in the covalently bonded semiconductors Si, Ge, GaAs, GaP, AlP, and ZnTe. The results are computed for deep levels transforming according to both A1 (s-like) and T2 (p-like) symmetries induced by substitutional impurities in the selected materials.

Deep level impurities under optical excitation are shown schematically in Figure 1.1. Case 1 occurs when an electron of energy  $E$  is driven from an initially full valence band to a deep level in the bandgap,  $E_d$ , which is initially empty. The energy required to cause this transition comes from a photon energy of  $h\nu_1$ . This process is called "absorption" since the material absorbs the photon. In this case, an electron is trapped at the deep level, leaving a hole in the valence band.

For case 2, an electron of energy  $E$  is driven from an initially full deep level energy state,  $E_d$ , in the bandgap to an initially empty level in the conduction band. The energy causing this transition comes from a photon energy of  $h\nu_2$ . This process is also called "absorption" because a photon is absorbed. In this case, an electron is put into a level in the conduction band.

Case 3 illustrates the transition of an electron from an initially full conduction band to an initially empty deep level state in the bandgap with the release of a photon of energy  $h\nu_2$ . This process is called "emission" because a photon is emitted from the material. In this case, an electron makes a transition from the conduction band to a deep level in the bandgap. From the point of view of a hole in the valence band, this transition is analogous to that represented by case 2 except the hole, not the electron, is undergoing the transition. That is, a hole makes a transition from the deep level to the conduction band.

Case 4 is analogous to case 1 because an electron makes a transition from an initially full deep level state,  $E_d$ , into a state in the valence band. This transition emits a photon of energy  $h\nu_1$ . This process is thus also called



"emission." From the hole viewpoint, a hole makes a transition from the valence band to the deep level.

A typical optical cross section for a deep level is illustrated in Figure 1.2. In this and subsequent optical cross section figures, the cross section is plotted on the electron energy scale with the zero of energy at the top of the valence band. The bandgap is indicated by the gap between the valence band edge and the conduction band edge. The intensity of the curve of an optical cross section represents the probability of an electron transition occurring with a given photon energy.

Again, consider case 1. The electron energy is represented by  $E$  in Figure 1.2. There is a probability that a transition will occur which will move the electron from its state in the valence band to a deep energy level,  $E_d$ , under the influence of a photon of energy  $h\nu_1$ . This probability is shown as  $P_1$ .

From conditions represented by case 2, the electron, represented by energy  $E_d$ , will make a transition from its current deep level state in the bandgap to an energy state in the conduction band,  $E$ , under the influence of a photon of energy  $h\nu_2$ . The probability of this transition occurring is shown as  $P_2$ .

Current use of the terminology "deep level" has evolved to define a level as "deep" if it is produced by the central cell potential alone, neglecting the Coulomb potential, regardless of its actual depth. In this thesis we adopt this definition exclusively. Thus, following Hjalmanson et al. (5, 6), in what follows, we neglect the Coulomb potential entirely. Therefore, in this description all impurity energy levels in the bandgap are "deep" and there are no shallow hydrogenic-like levels in this theory. The shallow, effective mass-like levels which result from the Coulomb potential could be included, in principle, in the theory in a straightforward but tedious manner. Since we desire to study deep levels here, we leave them out of our theory. Further discussion of these points may be found in Chapter II.

Optical studies of deep levels in semiconductors measure the electronic structures of the defects which produce such levels. Numerous studies have

been made to determine which defects form deep levels, or deep traps (2, 5, 7, 8).

The earliest models of defects in semiconductors, such as the hydrogenic model (otherwise known as effective mass theory, or EMT) (9, 10, 11, 12) do a reasonably accurate job of describing shallow impurity levels. However, they fail to describe deep levels, even qualitatively (13, 14, 15).

There have been several attempts to provide a theoretical description of the physics of deep level impurities (5, 6, 16, 17, 18). In this thesis, we use a method which is known collectively as the Vogl-Hjalmarson theory. This approach describes the host bandstructure using the  $sp^3s^*$  semi-empirical tight binding model of Vogl et al. (6) and the deep levels are described using the Hjalmarson et al. deep level theory (5, 19). We use this approach here because our main goal in this thesis is to provide a description of the chemical trends in the deep level optical cross sections as a function of both impurity and host.

Since it is very difficult to predict the energy level of any deep level impurity with accuracy, it is of more interest to study the chemical trends of deep levels in semiconductors. As shown by Hjalmarson et al. and Vogl et al., the major chemical trends in deep level energies may be determined by the energy bands of the undisturbed host and by the impurities' atomic structure. The Vogl-Hjalmarson theory has previously been extremely successful in its predictions of such trends for several defects in numerous semiconductor materials (20, 21, 22, 23, 24). Thus, it is ideally suited for application to the prediction of the chemical trends we desire here.

It should be emphasized that the formalism for the optical cross section that we derive in Chapter III is independent of our choice of bandstructure model and, with only relatively minor changes, it can also be used with an alternative deep level theory. Of course, the numerical results in this thesis do depend on our choice of both the bandstructure model and deep level theory.

Other approaches to the theory of deep levels exist (9, 11, 17, 18, 25, 26, 27, 28). Some examples are Jaros' theory (17, 27, 28) which uses pseudo-potentials, the Koster-Slater technique (29) and the semi-empirical cluster

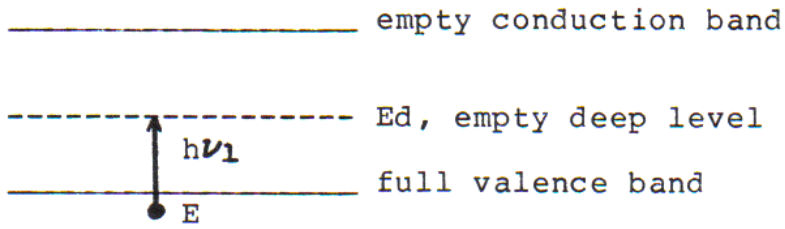
method. Other deep level theories are discussed in the literature (30 through 46).

The theory of optical cross sections of deep levels has received less attention than the deep level theory itself. The Lucovsky model (16) and the hydrogenic model have both been used to describe this cross section. The hydrogenic model gives excellent information concerning shallow levels of impurities, but the cross sections are not adequate for describing deeper levels. The Lucovsky model is also useful, except that it is limited to deep levels near the center of the bandgap.

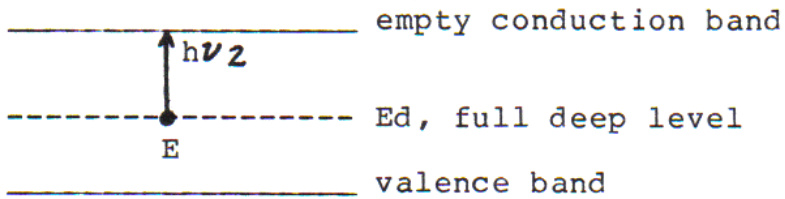
Jaros and co-workers also introduced a model describing optical cross sections of deep levels (17, 27, 28). This model is based on pseudo-potentials and a defect wave function calculated by Banks, Brand and Jaros using the Green's function method (28, 47, 48, 49).

The following chapters of this thesis are organized in such a manner as to logically develop results and conclusions. Chapter II discusses the applicable theories required for an understanding of optical cross sections. Chapter III develops the formalism for the optical cross section of a deep level produced by a substitutional impurity, on which numerical analysis is performed. Chapter IV analyzes the results of the numerical treatment of the optical cross sections and discusses the calculated chemical trends. Finally, Chapter V summarizes the analysis and chemical trends.

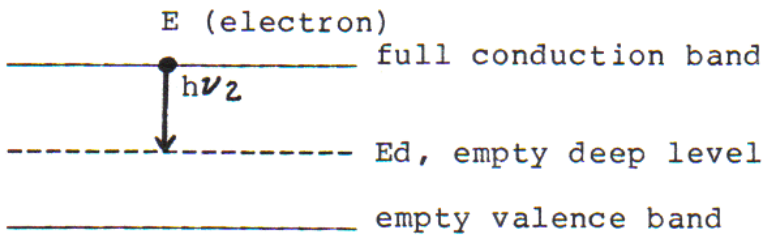
**Figure 1.1 Energy Levels**



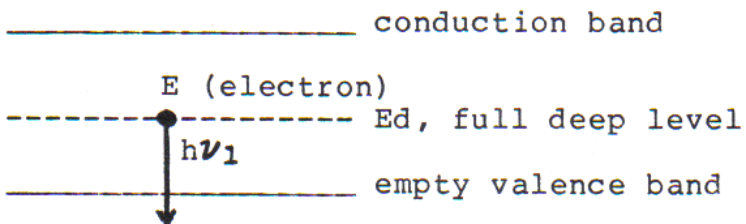
CASE 1 (ABSORPTION)



CASE 2 (ABSORPTION)

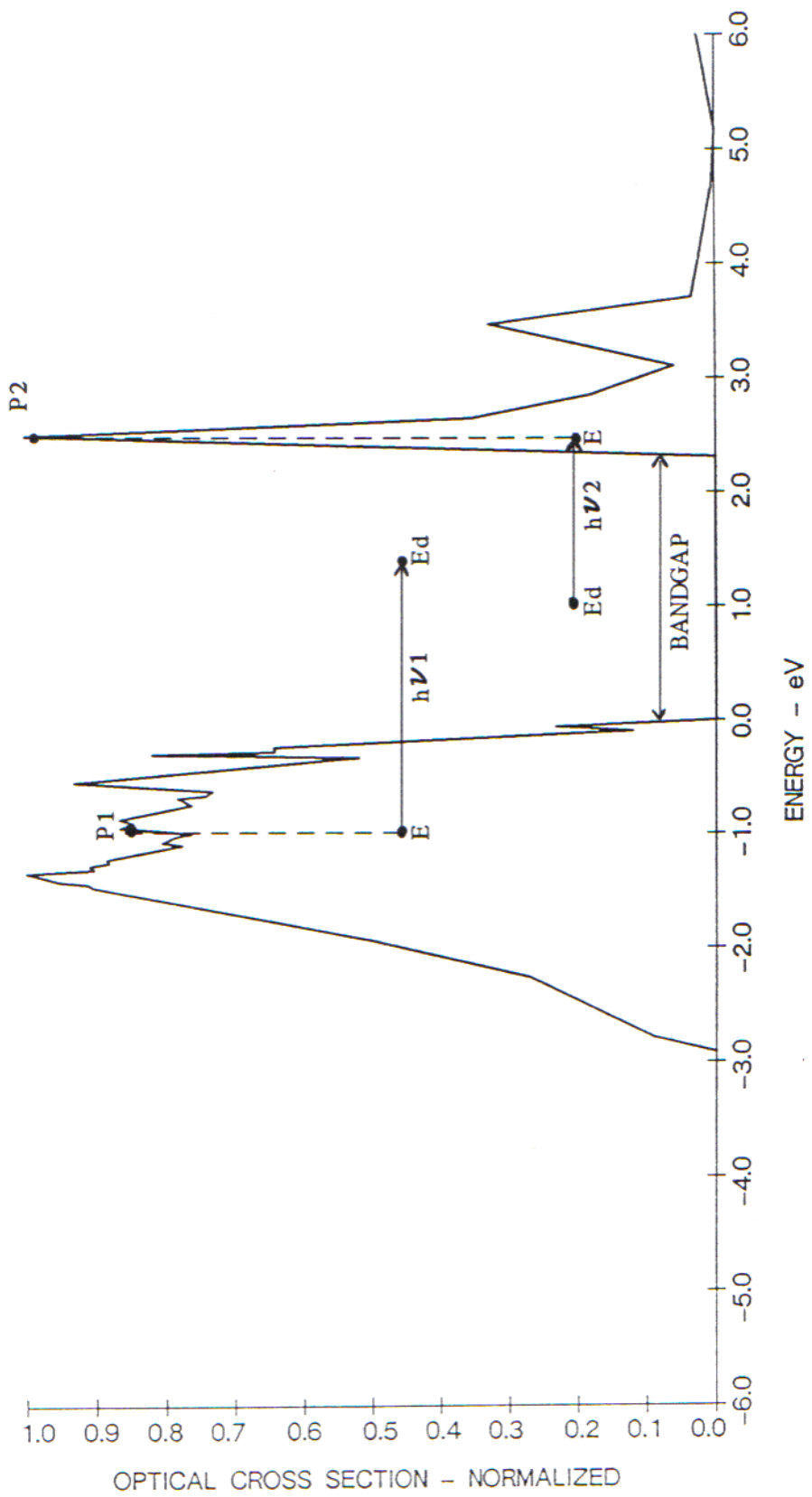


CASE 3 (EMISSION)



CASE 4 (EMISSION)

**Figure 1.2 Optical Cross Section of a Typical Semiconductor**



## CHAPTER II

### BACKGROUND

In this thesis, we develop a formalism for the deep level optical cross section which is in the spirit of the Lucovsky model (16) in that it assumes a short ranged defect potential only. However, our theory accurately takes into account the host bandstructure and enables one to straightforwardly obtain chemical trends by using the defect potential of Hjalmarson et al. (5, 6, 19, 50). Unlike the Lucovsky's model, the results in the present case must be obtained numerically. However, our theory is still computationally simple enough to enable us to obtain the desired trends with minimal computational effort.

There are two alternative definitions of a deep impurity level in the literature. Experimentally, impurity levels are considered "deep" if their distance from the band edges is large compared to  $K_b T$  at room temperature (where  $K_b$  is Boltzman's constant) (14). In this case, typically, one considers a level to be "deep" if it occurs at an energy which is greater than about 0.1 eV from a bandedge. Theoretically, an impurity energy level is called "deep" if the long range (Coulombic) potential can be neglected in comparison to the short range (central cell) potential, independent of the depth of the level in the bandgap (1, 5, 14, 17). In this chapter and in the rest of this thesis, we use the latter definition exclusively.

In this chapter we will briefly review some of the background material which is necessary to develop our formalism. Specifically, the elementary theory of shallow levels in semiconductors, the particular version of tight binding bandstructure theory that we use, a semi-empirical theory of deep levels, and the Lucovsky model for the deep level optical cross section are all briefly reviewed. The physics of shallow levels is also contrasted to that of deep levels.

#### **2.1 Hydrogenic Model For Shallow Levels**

The hydrogenic, or effective mass model, (derived from the effective mass theory, EMT) is one of the earliest theories of defects in semiconductors (9, 10,



11, 12, 16). The simplest version of this theory is easily understood. Assume, for example, that N electrons occupy the valence bands of the host material along with an impurity whose valence differs from that of the replaced host atom by +1 (one extra electron and one extra proton). Assume also, that the material of interest is a covalent material with four  $sp^3$  hybrid bonds per atom. The extra electron will occupy the lowest energy state available to it. For small k (especially near the Brillouin center where  $k \sim 0$ ), one can always write the energy of the lowest conduction band as

$$E(\mathbf{k}) = \frac{E_C + \hbar(\mathbf{k})^2}{2 m_e^*} \quad , \quad (2.1)$$

where  $E_C$  is the conduction band minimum and the effective mass,  $m_e$  is defined as

$$\frac{1}{m_e^*} = \frac{1}{\hbar^2} \cdot \frac{d^2 E(\mathbf{k})}{d \mathbf{k}^2} \quad (2.2)$$

The impurity atom has one extra valence electron and one extra proton. The extra electron is not taken up in the four bonds, so that it is only weakly bound to the proton and is free to move about in the crystal (it goes into the conduction band). The host atoms are, on the average, neutral but since the electron is far from the proton, the impurity atom has an effective positive charge. This sets up a Coulombic field in addition to the other crystal fields that existed before the introduction of the impurity. The electron is weakly bound to the proton through this Coulomb potential. It can now be viewed as a "free electron" with mass,  $m_e^*$ , which is acted upon by the Coulombic field. Furthermore, this Coulomb field is screened by the dielectric constant of the material. Thus the problem of finding the energy levels of the impurity is analogous to that of the hydrogen atom with the proton having a charge equal to  $e/\sqrt{\epsilon}$ , where  $\epsilon$  is the

dielectric constant of the material, and with the electron having a mass,  $m_e^*$ . Since the hydrogen atom has bound states below the ionization continuum, the bound states for the electron are introduced below the conduction band edge, with energies given by

$$E_n = E_c - e^4 m_e^* / (2\hbar^2 \epsilon^2 n)^2 , \quad (2.3)$$

where  $n = 1, 2, 3, \dots$

The energy levels of the hydrogen atom are

$$E_n^H = - e^4 (m_0) / (2\hbar^2 n)^2 , \quad (2.4)$$

where  $m_0$  is the mass of the free electron. Equation (2.3) can thus be written as

$$E_n = E_c + E_n (m_e^* / m_0 \epsilon^2) . \quad (2.5)$$

Such impurities are called donors and the associated energy levels are called donor levels. Typical values of  $\epsilon$  are of the order of 10, and experimental values of  $m_e$  range from about  $0.03m_0$  to about  $m_0$ . Equation (2.3) thus shows that the ionization energy of the lowest donor energy level ( $n=1$ ) is of the order of  $100 m_e V$ . Compared with the bandgaps of materials discussed in this thesis, which range from about 1 eV to about 3 eV, these donor ionization energy levels are therefore clearly shallow.

A similar approach will work for impurities whose valence differs from that of the replaced host atom by -1 (one fewer electron and proton). The resulting hydrogenic levels are, in this case, introduced above the top of the valence band and are called acceptor levels. In this case, Eq. (2.5) becomes

$$E_n = E_v - E_n^H (m_h^* / m_0 \epsilon^2) \quad , \quad (2.6)$$

where  $E_v$  is the valence band maximum and  $m_h$  is the effective mass of a hole at the top of the valence band.

The hydrogenic model of shallow impurity levels is valid for the description of defects which introduce Coulombic potentials in the crystal (i.e., those that are nonisovalent). Depending on the complexity of the band structures and the values for  $m_e$  and  $\epsilon$ , the results of this model in comparison with data vary from excellent to poor. It works best for simple, or single donors or acceptors, but can be extended to double donors or acceptors. It also works well for excited states and less well for the description of the impurity associated ground state (15).

## **2.2 Vogl's Tight Binding Theory For Host Bandstructures**

The nearest neighbor tight binding bandstructure model for zincblende and diamond materials used in our optical cross section calculations was developed by Vogl et al.(6). It has been used extensively in other applications to study the electronic properties of semiconductors (51, 52, 53). This model constructs the required energy bands for  $sp^3$ -bonded semiconductors by using only 13 semi-empirical parameters. Prior nearest neighbor tight binding models were not able to adequately fit the conduction bands for indirect gap semiconductors. Vogl et al. circumvented this difficulty by including an excited state on each atom at high energy (called the  $s^*$  state), which serves to push down the lowest conduction bands at the proper points in the Brillouin zone (54, 55). This  $s^*$  state is somewhat of an artifact of the theory which attempts to simulate the higher lying d states which should actually be present. It was introduced to push down the energy eigenvalues to lower energies. The resulting conduction bands are in good agreement with both experiment and more sophisticated theory. Theories with fewer than eight bands cannot adequately describe the chemistry of covalently bonded materials. However, the inclusion of the excited  $s^*$ -state on

each atom gives us an  $sp^3s^*$  basis and a ten-band theory. Therefore, using this theory, we can describe all energy bands, even the lowest conduction bands that were not available in the prior models. In an  $sp^3$  basis and in the nearest-neighbor approximation there are four diagonal matrix elements and five independent nearest-neighbor transfer matrix elements. The excited  $s^*$ -state couples only to the p-states on adjacent sites and does not couple to the s-states on different sites. This introduces four additional matrix elements. All such matrix elements in the Vogl et al. theory were empirically fit to a combination of experiment and accurate pseudo-potential bandstructures (6, 56). The empirical matrix elements in the Vogl et al. model are derived and discussed in detail in Reference 6 where the numerical values are also listed.

There are other nearest neighbor tight binding models, some of which motivated the Vogl et al. theory. One such model is the empirical Bond Orbital Model developed by Harrison and co-workers (57, 58, 59, 60, 61). This model provides a simple nearest neighbor tight binding theory of valence bands. With this model, one can estimate the nature of the filled valence bands of almost any semiconductor. However, this model does not accurately address the empty conduction band states, and for it to be usable for our purposes, a comparable description of the conduction states is required. Vogl et al. refer to Chadi's model (62) but this model fails to describe the lowest conduction bands. This causes this model not to produce the indirect fundamental bandgap for the indirect gap semiconductors.

### **2.3 Hjalmarson's Deep Level Theory**

The version of deep level theory we use in this thesis was developed by Hjalmarson et al. (5, 19). This theory predicts deep level energies using only host and impurity atomic orbital energies (ionization energies) and the Vogl et al. tight binding bandstructure (discussed in Section 2.2 above) for the host material. This approach and its generalizations have successfully predicted the chemical trends for numerous defect/host systems (5). For example, see Refs. 24, 52, 63,

64, 65, 66, 67, 68, 69, 70, 71. The general defect potential for substitutional defects has several contributions: a short range central cell potential, long range Coulomb potential and an electron-lattice interaction caused by distorting the lattice near the impurity (72). In the Hjalmarson et al. approximation, only the short range, central cell potential is kept, since it is known that deep levels are controlled primarily by this contribution. Thus, all levels in this theory are "deep" in the sense described in Chapter I (73). As stated above, Hjalmarson et al. developed their deep level theory in conjunction with the Vogl et al. semi-empirical tight-binding,  $sp^3s^*$ , ten-band model. Since the excited s-like states are generally in the same energy range for all  $sp^3$ -bonded semiconductors, a substitutional impurity for a host atom will cause very little change in them. Therefore, the defect potential in the Hjalmarson theory is determined only by the s- and p-like ionization energies. In this approximation, this potential is a one site potential with no lattice relaxation; it is thus a diagonal matrix. In this theory, the matrix elements are proportional to the difference between atomic energies of the host and the impurity. Hjalmarson et al. make three approximations concerning the form of the defect potential. These are (i) that the atomic energy difference between two atoms in a solid is similar to that difference for two free atoms, (ii) that the difference of the interatomic matrix elements is very small (generally they are set to zero), and (iii) lattice relaxation and charge state splittings are neglected. These have been included in later generalizations of the theory (66, 74).

#### **2.4 Lucovsky's Model For Optical Cross Sections of Deep Levels**

In order to develop a theory for optical cross sections of deep levels, Lucovsky (16) made the approximation that the deep level impurity potential is a delta-function well. That is, in this theory, this potential is infinitely deep and infinitely short ranged. Based on this approximation, Lucovsky derived an expression for the cross section using the dipole approximation and time dependent perturbation theory (17). The derivation of the Lucovsky cross section

is detailed in the literature (16). This cross section  $\sigma(\hbar\nu)$  (for the conduction band only) has the following form

$$\sigma(\hbar\nu) = (\text{constant}) \frac{(E_i)^{(1/2)}(\hbar\nu - E_i)^{(3/2)}}{(\hbar\nu)^3} \quad (2.7)$$

where  $\hbar\nu$  is the photon energy and  $E_i$  is the deep level (ionization) energy. The constant contains parametric characteristics of the material, such as the index of refraction and the effective field ratio for the induced transition. Because this constant is independent of photon energy and deep level energy, it is unimportant for the general functional form of the Lucovsky model.

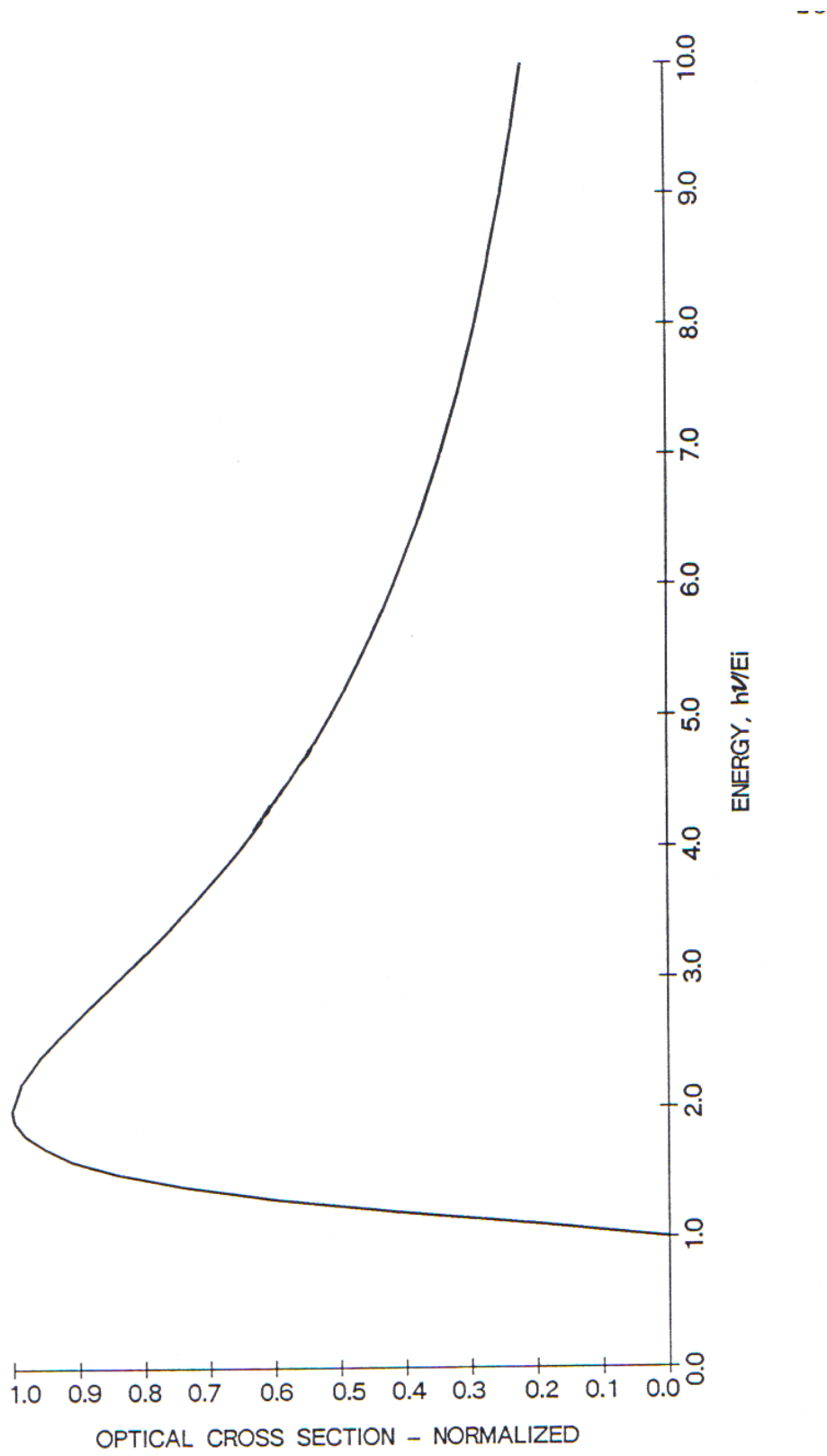
The function of Eq. (2.7) has certain qualitative characteristics as a function of the photon energy. At  $\hbar\nu = E_i$  it rises from zero and has a maximum at  $\hbar\nu = 2E_i$ . It falls off approximately as  $\hbar\nu^{(-3/2)}$  for  $\hbar\nu \gg E_i$ . This behavior is illustrated in Figure 2.1. In this case, the cross section is plotted as a function of photon energy  $\hbar\nu$

. For the valence band, the cross section is a mirror image of that of Figure 2.1.

Lucovsky's model is simple because it obtains the cross section in closed form. However, it can only predict the threshold, the transition maximum and the general shape of the cross section. This model does not take into account the effects of the host bandstructure nor does it allow one to obtain chemical trends, as it predicts a universal cross section shape for all deep levels.

The results of applying Lucovsky's model to the deep level optical cross sections in a specific material selected in this thesis are discussed in detail in Chapter IV.

**Figure 2.1. Lucovsky's Model For Optical Cross Sections of Deep Levels, Conduction Band Only.**





**CHAPTER III**  
**FORMALISM FOR THE OPTICAL CROSS SECTION**

**3.1 Derivation of the General Form**

The starting point for our deep level optical cross section formalism is time dependent perturbation theory from quantum mechanics (75). Specifically, we use "Fermi's Golden Rule" for the probability per unit time of a perturbation inducing a transition from one stationary state to another. Let  $n$  be the initial state and  $m$  be the final state. From first order time dependent perturbation theory, the probability that a perturbation will induce a transition from the state  $n$  into the state  $m$  with energy difference  $\hbar \omega_{nm} = E_m - E_n$  during the time in which the perturbation occurs is given by

$$T_{nm}(\tau) = \frac{1}{\hbar^2} \left| \int_0^\tau \langle n | \hat{W} | m \rangle e^{(i\omega_{nm})t} dt \right|^2 \quad (3.1)$$

where  $\tau$  is the period of the perturbation,  $t$  is the time at which the transition occurs,  $\omega$  is the frequency of the perturbation and  $\langle n | \hat{W} | m \rangle$  is the matrix element of the perturbation between the initial and final states. If the perturbation is constant, the matrix element  $\langle n | \hat{W} | m \rangle$  does not depend on time and the integral can easily be evaluated. It becomes

$$\int_0^\tau \langle n | \hat{W} | m \rangle e^{(i\omega_{nm})t} dt = \langle n | \hat{W} | m \rangle \frac{e^{(i\omega_{nm})t} - 1}{i\omega_{nm}} \quad (3.2)$$

The transition probability during the period that the perturbation occurs, by combining Eqs . (3.1) and (3.2), can easily be found to be

$$T_{nm}(\tau) = \frac{2}{\hbar^2} \left| \langle n | \hat{W} | m \rangle \right|^2 F(E_n - E_m), \quad (3.3)$$

where

$$F(E_n - E_m) = \frac{1 - \cos [(E_n - E_m)\tau / \hbar]}{[(E_n - E_m)^2 \tau / \hbar]}. \quad (3.4)$$

When  $E_n = E_m$ , the function  $F(E_n - E_m)$  has a maximum value of  $1/2 \tau^2$ . This function vanishes for  $|E_n - E_m| = 2\pi\hbar / \tau, 4\pi\hbar / \tau, \dots$ . For small values of  $\tau \ll \hbar / E_n$ , the transition probability is proportional to  $\tau^2$ . If  $\tau$  is sufficiently large compared to the period  $\hbar / (E_n - E_m)$  of the system,  $F(E_n - E_m)$  can be approximated as a delta function

$$F(E_n - E_m) = \pi \tau \hbar \delta(E_n - E_m). \quad (3.5)$$

In this case, Eq. (3.3) for the transition probability can be rewritten in the form

$$T_{nm}(\tau) = \frac{2}{\hbar^2} \left| \langle n | \hat{W} | m \rangle \right|^2 \tau \delta(E_n - E_m). \quad (3.6)$$

Since the transition probability is proportional to the time during which the perturbation occurs, the transition probability per unit time or the number of transitions per second, can be written as

$$P_{nm} = T_{nm}(\tau) = \frac{2\tau}{\hbar} \left| \langle n | \hat{W} | m \rangle \right|^2 \delta(E_n - E_m). \quad (3.7)$$

This result is commonly known as "Fermi's Golden Rule."

Under the action of a perturbation which is periodic in time, transitions take place to states with energies satisfying the condition  $E_m = E_n + \hbar\omega$ , where  $\omega$  is

the frequency of the perturbation. In our case, we are concerned with an external electromagnetic (photon) field of frequency  $\omega$ .

Now let us assume that the quantum system described by Eq. (3.7) is interacting with electromagnetic radiation of frequency  $\omega$ . In this case, from standard quantum mechanics, the perturbation operator,  $\hat{W}$ , is

$$\hat{W} = \frac{-e}{\mu c} (\hat{A} \cdot \hat{p}), \quad (3.8)$$

where  $e$  is the charge of the particle,  $\mu$  is the electron mass,  $c$  is the speed of light,  $3 \times 10^8$  m/s, and  $\hat{A}$  is the vector potential (17), which has the form

$$\hat{A} = A_0 [\exp i(\vec{k} \cdot \vec{r} - \omega t)] + \text{const.} \quad (3.9)$$

In Eq. (3.8),  $\hat{p}$  is the momentum operator. If Eq. (3.8) is used in Eq. (3.7), the resulting transition probability is said to be calculated in the dipole approximation. In this case, the matrix element  $\langle n | \hat{W} | m \rangle$  is clearly proportional to the momentum matrix element  $\langle n | \hat{p} | m \rangle$ .

In order to derive the general form of the optical cross section, we must first choose a specific initial state (say the valence band, of energy  $E_{n, \vec{k}}$ ), a specific final state (say a deep level of energy,  $E_i$ ), and photon energy,  $h\nu$ , and sum over all initial states ( $\psi_{n, \vec{k}}$ ). In the calculation discussed below, the final (or initial) state is given by the impurity wavefunction,  $\psi$ , which is expanded in terms of the unperturbed host crystal eigenfunctions,  $\phi_{n, \vec{k}}$ , discussed later in this section, and the initial (or final) state is a particular bandstate with wavefunction,  $\phi_{n, \vec{k}}$ . Substituting those, along with Eqs. (3.8) and (3.9) into Eq. (3.7), using the dipole approximation as derived by Dexter (76) and Blakemore (77), and summing over all initial (band) states gives the general form for the optical cross section  $\sigma(h\nu)$  of a deep level impurity in a semiconductor

$$\sigma(h\nu) = (\text{constant} / \hbar) \sum_n^{\vec{k}} \left| \langle \psi | \hat{p} | \phi_{n, \vec{k}} \rangle \right| \delta(|E_i| + E_{n, \vec{k}} - h\nu) \quad (3.10)$$

where  $h\nu$  is the photon energy,  $|\psi\rangle$  is the localized impurity wave function,  $\hat{p}$  is the momentum operator,  $|\phi_{n, \vec{k}}\rangle$  is the host crystal eigenfunction (band wave function), or Bloch function,  $n$  is a band index,  $\vec{k}$  is a wave vector in the first Brillouin zone,  $E_i$  is the impurity deep level energy, and  $E_{n, \vec{k}}$  is a band energy. The constant contains material dependent parameters and is independent of the

photon energy. Therefore, it makes no contribution to the general shape of the optical cross section.

### **3.2 Form of the Cross Section in Deep Level Theory**

The goal of the following derivation is to begin with Eq. (3.10) and to obtain a form for  $\sigma(h\nu)$  which can be easily numerically evaluated and which uses some of the results of deep level theory in its derivation (17, 77). It should be noted that the electron-phonon interaction is not considered in the formalism we discuss here. Although, in an experimental cross section, such effects are well-known to be present, the following theory neglects this contribution and considers pure electronic transitions only. In order for our results to be compared to experiment, it would therefore be necessary to extract the phonon contribution from the experimental results. A method for doing this is outlined in Ref. 72.

The wavefunction of a deep level localized state in the band gap of a semiconductor can be expanded in terms of Bloch functions (the eigenfunctions of the host crystal Hamiltonian) (17),

$$|\psi\rangle = \sum_n^{\vec{k}} A_{n, \vec{k}} |\phi_{n, \vec{k}}\rangle, \quad (3.11)$$

where  $H^0 |\phi_{n, \vec{k}}\rangle = E_{n, \vec{k}} |\phi_{n, \vec{k}}\rangle$ ,  $A_{n, \vec{k}}$  is the expansion coefficient (14, 28, 78), and  $H^0$  is the host Hamiltonian.

Now consider the quantum mechanical problem of solving the one-electron Schrodinger equation in the presence of the deep level defect,

$$H |\psi\rangle = E |\psi\rangle, \quad (3.12)$$

where  $H$  is the Hamiltonian and  $E$  is the energy eigenvalue. In the presence of a deep level impurity, one can write

$$H = H^0 + V \quad , \quad (3.13)$$

where  $H^0$  is the perfect crystal hamiltonian and  $V$  is the impurity potential. Thus,

$$(H^0 + V) |\psi\rangle = E|\psi\rangle \quad .. \quad (3.14)$$

This can be rearranged in the form

$$V|\psi\rangle = (E - H^0) |\psi\rangle \quad . \quad (3.15)$$

Rearranging again yields

$$(E - H^0)^{-1} V|\psi\rangle = |\psi\rangle \quad . \quad (3.16)$$

Using the definition of the host Green's function (79, 80)

$$G^0(E) = (E - H^0)^{-1} \quad , \quad (3.17)$$

Eq. (3.16) can be written as

$$G^0(E) V|\psi\rangle = |\psi\rangle \quad . \quad (3.18)$$

The advantage of writing Schrodinger's equation in this form is that it is only necessary to solve it in real space in the subspace of the impurity potential  $V$ . For deep level impurities  $V$  is very short ranged, as already discussed. Substituting Eq. (3.11) into the right hand side of Eq. (3.18) yields,

$$G(E) V|\psi\rangle = \sum_{\vec{k}} A_{n, \vec{k}} |\phi_{n, \vec{k}}\rangle . \quad (3.19)$$

Matrix elements of this equation in the Bloch representation are

$$\langle \phi_{n', \vec{k}'} | G(E) V |\psi\rangle = \sum_{\vec{k}} A_{n, \vec{k}} \langle \phi_{n', \vec{k}'} | \phi_{n, \vec{k}} \rangle . \quad (3.20)$$

The Bloch functions are orthonormal so that

$$\langle \phi_{n', \vec{k}'} | \phi_{n, \vec{k}} \rangle = \langle \delta_{n', \vec{k}'} | \delta_{n, \vec{k}} \rangle . \quad (3.21)$$

Using Eq. (3.21) in Eq. (3.20) yields an expression for the coefficients,  $A_{n, \vec{k}}$ , which has the form

$$A_{n, \vec{k}} = \langle \phi_{n, \vec{k}} | G(E) V |\psi\rangle . \quad (3.22)$$

Since  $H^0 |\psi_{n, \vec{k}}\rangle = E_{n, \vec{k}} |\psi_{n, \vec{k}}\rangle$  it can be easily shown that

$$\langle \phi_{n, \vec{k}} | G(E) = \langle \phi_{n, \vec{k}} | \frac{1}{E - E_{n, \vec{k}}} . \quad (3.23)$$

Combining Eq. (3.22) and (3.23)

$$A_{n, \vec{k}} = \frac{\langle \phi_{n, \vec{k}} | V |\psi\rangle}{E - E_{n, \vec{k}}} . \quad (3.24)$$

Now let us write the matrix element occurring in Eq. (3.10) utilizing the results from Eq. (3.11) and (3.24). From Eq. (3.11), it can be seen that

$$\langle \psi | \hat{p} | \phi_{n, \vec{k}} \rangle = \sum_{n'}^{\vec{k}'} (A_{n', \vec{k}})^* \langle \phi_{n', \vec{k}'} | \hat{p} | \phi_{n, \vec{k}} \rangle . \quad (3.25)$$

Since a reasonable approximation is that

$$\hat{p} | \psi_{n, \vec{k}} \rangle = \hbar \vec{k} | \psi_{n, \vec{k}} \rangle \quad \text{and since the Bloch functions are}$$

orthonormal, this becomes

$$\langle \psi | \hat{p} | \phi_{n, \vec{k}} \rangle = \hbar \vec{k} (A_{n, \vec{k}})^* . \quad (3.26)$$

Using Eq. (3.24), the matrix element which enters the cross section becomes

$$\langle \psi | \hat{p} | \phi_{n, \vec{k}} \rangle = \frac{\hbar \vec{k} \langle \psi | V | \phi_{n, \vec{k}} \rangle}{E - E_{n, \vec{k}}} . \quad (3.27)$$

As has already been discussed, in the Hjalmarson deep level theory the defect potential  $V$  is assumed to be diagonal in a site representation basis and localized in the central cell at the origin (5, 81) . It has the form

$$V = \sum_{1\beta} | 1, \vec{0}, \beta \rangle V_{1\beta} \langle 1, \vec{0}, \beta | . \quad (3-28)$$

Here, 1 stands for the irreducible representation of the defect level, either A1 (s-like) or T2 (p-like) , and  $\beta$  is a site designator. In our notation,  $\beta = 0$  (1) for an impurity at the anion (cation) site. Therefore, the form for Eq. (3.27) in the Hjalmarson et al . deep level theory is



$$\begin{aligned}
\langle \psi_{1\beta} | \hat{p} | \phi_{n, \vec{k}} \rangle = \\
\hbar \vec{k} \langle \psi_{1\beta} | \sum_{1'\beta'} \frac{| 1', \vec{0}, \beta' \rangle V_{1\beta} \langle 1', \vec{0}, \beta' | \phi_{n, \vec{k}} \rangle}{E_{1'\beta'} - E_{n, \vec{k}}} , \quad (3.29)
\end{aligned}$$

where  $\psi_{1\beta}$  means the wavefunction of symmetry 1 for the deep level of energy  $E_{1\beta}$  for an impurity at site  $\beta$ . Because of orthogonality we have,

$$\langle \psi_{1\beta} | 1', \vec{0}, \beta' \rangle = \delta_{11'} \delta_{\beta\beta'} \langle \psi_{1\beta} | 1, \vec{0}, \beta \rangle . \quad (3.30)$$

This yields a new form for Eq. (3.27), which is

$$\begin{aligned}
\langle \psi_{1\beta} | \hat{p} | \phi_{n, \vec{k}} \rangle = \\
\hbar \vec{k} V_{1\beta} \langle \psi_{1\beta} | 1, \vec{0}, \beta \rangle \langle 1, \vec{0}, \beta | \phi_{n, \vec{k}} \rangle . \quad (3.31)
\end{aligned}$$

Following Hjalmarson's dissertation (5), the host wave functions are determined entirely by matrix elements of the host Hamiltonian in a basis of orthonormal atomic orbitals. Thus we write

$$| \phi_{n, \vec{k}} \rangle = \sum_{1\beta} C_{\vec{k}, n, 1\beta} | \Phi_{1\beta, \vec{k}} \rangle , \quad (3.32)$$

where  $\Phi_{1\beta, \vec{k}}$  is the atomic wavefunction for covalently bonded orbitals in the mixed Bloch-Wannier basis and  $C_{\vec{k}, n, 1\beta}$  are eigenvectors of the Hamiltonian.

Also, from Hjalmarson's dissertation (5), the functions  $\Phi$  are given in terms of localized atomic orbitals at a given lattice site by

$$| \Phi_{1\beta} \vec{k} \rangle = N^{(1/2)} \sum_{i\vec{R}} \exp i \vec{k} \cdot ( \vec{R} + \beta\tau_i ) | 1, \vec{R}, \beta \rangle . \quad (3.33)$$

where  $\tau_i$  are the positions of the four atoms nearest to a central anion (See Appendix A) . That is, the functions  $\Phi$  are basically the fourier transforms of the atomic orbitals at each site. Utilizing Eq.(3.32) and (3.33), the quantity

$\langle 1, \vec{0}, \beta | \phi_{n, \vec{k}} \rangle$  occurring in Eq. (3.31) can be written as

$$\langle 1, \vec{0}, \beta | \phi_{n, \vec{k}} \rangle = \sqrt{N} \sum_{1'\beta'i} \exp [ i \vec{k} \cdot ( \vec{R} + \beta\tau_i ) ] C_{\vec{k}, n, 1\beta} \langle 1, \vec{0}, \beta | 1, \vec{0}, \beta \rangle , \quad (3.34)$$

Since the site representation basis is orthonormal, we have

$$\langle 1, \vec{0}, \beta | 1, \vec{R}, \beta \rangle = \delta_{11'} \delta_{\vec{R} \vec{0}} \delta_{\beta\beta'} . \quad (3.35)$$

Eq. (3.34) thus reduces to

$$\langle 1, \vec{0}, \beta | \phi_{n, \vec{k}} \rangle = \sum_i \exp ( i \vec{k} \cdot \beta\tau_i ) C_{\vec{k}, n, 1\beta} . \quad (3.36)$$

Substituting Eq. (3.36) into Eq. (3.31) gives

$$\langle \psi_{1\beta} | \hat{p} | \phi_{n, \vec{k}} \rangle = \frac{\hbar \vec{k} \cdot \mathbf{V}_{1\beta}}{E_{1\beta} - E_{n, \vec{k}}} \langle \psi_{1\beta} | 1, \vec{0}, \beta \rangle \left[ \sum_i \exp ( i \vec{k} \cdot \beta\tau_i ) C_{\vec{k}, n, 1\beta} \right] \quad (3.37)$$

$$\sqrt{N} E_{1\beta} - E_{n, \vec{k}}$$

Substituting Eq . (3.37) into the general equation for the cross section, Eq. (3.10) yields

$$\sigma_{1\beta}(h\nu) = \frac{\text{constant } V_{1\beta}^2 | \langle \psi_{1\beta} | 1, \vec{0}, \beta \rangle |^2}{\hbar N} \times \quad (3.38)$$

$$\sum_{n, \vec{k}} \frac{\vec{k}^2 | \sum \exp(i \vec{k} \cdot \beta \tau_i) |^2 | C_{\vec{k}, n, 1\beta} |}{E_{1\beta} - E_{n, \vec{k}}} .$$

The shape of the optical cross section of the deep level is not affected by the constant in Eq. (3.38) which consists of parameters which are characteristic of the material of interest. These parameters, such as the index of refraction and the field ratio for the induced transition, are independent of photon energy and the deep level impurity energy.

Here we seek trends in the cross section as a function of deep level energy. In this regard, Ren, Hu, Sankey, and Dow (81) have shown that the deep level wavefunction  $\langle \psi_{1\beta} | 1, \vec{0}, \beta \rangle$  is approximately independent of the deep level energy. Thus in what follows, we utilize their results and make the approximation that

$$| \langle \psi_{1\beta} | 1, \vec{0}, \beta \rangle |^2 = \text{constant independent of energy.} \quad (3.39)$$

The final form of the optical cross section which we use in this thesis is thus given by

$$\sigma_{1\beta}(h\nu) = (\text{constant} / \hbar) (V_{1\beta}^2 / N) \sum_{n, \vec{k}} \vec{k}^2 | \sum \exp(i \vec{k} \cdot \beta \tau_i) |^2 | C_{\vec{k}, n, 1\beta} |^2 \times \delta ( | E_{1\beta} | + E_{n, \vec{k}} - h\nu ) . \quad (3-40)$$

The quantities  $E_{n, \vec{k}}$  and  $C_{\vec{k}, n, 1\beta}$  can be calculated easily using the Vogl Hamiltonian and standard numerical techniques. These quantities as well as  $E_{1\beta}$  and  $V_{1\beta}$  are calculated in the program shown in Appendix B.

The optical cross section,  $\sigma_{1\beta}(h\nu)$ , Eq. (3.40), is in the form of a generalized density of states. Numerical methods for computing such functions were developed by Hjalmarson using a method based on that originally due to Lehman and Taut (5, 82). The computer program used to calculate  $\sigma_{1\beta}(h\nu)$  is therefore an extension of that developed by Hjalmarson. Both the program for the optical cross section and the related numerical analysis are described in detail in Appendices A and B.

## **CHAPTER IV**

### **RESULTS AND CHEMICAL TRENDS**

#### **4.1 Introduction**

In this chapter, for the materials selected, results for the computed optical cross section for various impurity levels in the bandgap are presented. In order to illustrate the chemical trends in this quantity as a function of impurity level, in each case three deep impurity levels were selected; one near the valence band edge, one near the center of the bandgap, and one near the conduction band edge. Also in this chapter, the optical cross sections for deep levels obtained by our theory are contrasted to those obtained in Lucovsky's model. Also, the trends of the Lucovsky model as a function of the deep level impurity are discussed for three different energy levels within the bandgap. The chemical trends in the optical cross section predicted by our theory as the semiconductor host is varied are also discussed in this chapter. In particular, the cross sections for materials of the zincblende and diamond structures and for materials with direct and indirect bandgaps are compared and contrasted. In addition, the effects of the level symmetry on the optical cross section are discussed. Finally, the optical cross sections of deep level impurities based on Jaros' theory are compared and contrasted with those obtained in the present theory. It should be noted that in our cross section curves, the zero of energy is taken as the top of the valence band.

#### **4.2 Comparison to Lucovsky's Model**

From the discussion of Lucovsky's model in Chapter II, one concludes that the this model is not adequate for describing the optical cross section unless the impurity level is very near the center of the bandgap (5, 16, 17). To illustrate an application of Lucovsky's model and compare it with our theory, we will examine the optical cross section for deep level impurities in Si. For this illustration, we

have chosen levels at 1.00 eV (near the conduction band edge), 0.75 eV (near the center of the bandgap), and 0.25 eV (near the valence band edge) in this material.

Figure 4.1 shows the results obtained when applying Lucovsky's model to these cases, for transitions to the conduction band only. In this case, the cross section is plotted as a function of normalized photon energy. As the impurity level changes from near the conduction band to near the valence band, the curves broaden as expected. In Lucovsky's model, the cross section maximum must occur at two times the value of the impurity energy. Accordingly, the peaks of the cross sections should occur at 0.50 eV (for  $E_i = 0.25$  eV), at 1.50 eV (for  $E_i = 0.75$  eV), and at 2.00 eV (for  $E_i = 1.00$  eV). However, our results for deep levels in Si, Figure 4.2, show that when the impurity level is near the conduction band edge (1.00 eV), the cross section peaks at approximately 1.51 eV, or 1.5 times the impurity energy. Also, in our theory, when the impurity level is near the valence band edge (0.25 eV), the cross section peaks at approximately 1.599 eV, or 6.4 times the impurity energy. Only for an impurity level near the center of the bandgap (0.75 eV) does Lucovsky's model yield results that are consistent with our theory, which is based on deep level theory. In this case, the cross section peaks at approximately 1.58 eV, or 2.11 times the impurity energy. It is also clear that the shapes of the optical cross section curves obtained in our theory and Lucovsky's model are very different.

Therefore, when compared to our theory, the Lucovsky model behaves as expected for Si. That is, the cross section broadens as the level becomes deeper (with respect to the conduction band edge). This model is thus only valid for levels that are near the center of the bandgap, where the cross section peaks at a value equivalent to two times the deep level impurity energy.

Although not discussed or illustrated in this thesis, a similar approach can be applied to the valence band with analogous results.

In Figure 4.2 and all subsequent figures, the cross section is plotted on the electron energy scale where the top of the valence band is taken as the zero of energy. Transformation to the photon energy scale can be made by utilizing the relation

$$h\nu = | E - E_i | \quad , \quad (4.1)$$

where  $E$  is the electron energy and  $E_i$  is the deep level energy.

### **4.3 Zincblende and Diamond Lattices**

Compound semiconductors which contain elements from columns III and V of the periodic table (83), such as GaAs, AlP, and GaP crystallize in the tetrahedrally coordinated zincblende lattice structure (47, 54, 84). Since they behave as semiconductors, their bandgaps are relatively small compared to those of insulators. The electrons in these materials are shared in covalent bonds between neighbors. Similarly, the elemental semiconductors from column IV of the periodic table, such as Ge and Si, crystallize in the tetrahedral diamond structure. Each atom shares  $sp^3$  bonds with four nearest neighbors of the same atom type, causing these materials to be extremely covalent.

In the elemental semiconductors (diamond structure), Si and Ge, only s-like deep levels, whose wavefunctions transform according to the A1 representation of the Td point group, have been considered because impurity levels in these materials are most often s-like (17, 28, 78). Similarly, it has been determined that impurity levels at the anion site in zincblende crystals often have wavefunctions which transform according to the A1 representation of the Td point group (17, 28, 78). Thus, the optical cross sections of deep levels transforming according to the A1 representation in the diamond and zincblende materials are compared and contrasted here.

For each zincblende and diamond material discussed and illustrated in this chapter, the computed cross section for transitions to both the conduction band and the valence band for the deep levels at three energies are shown.

The optical cross sections for A1-symmetric deep levels in Si, shown in Figure 4.2, and in Ge, shown in Figure 4.3, are typical of the results for the diamond structure semiconductors.

As can be seen in these figures, the cross sections for transitions to the conduction bands show a sharp rise near the band edge and, for impurity levels near the center of the bandgap, peak at an energy equal to approximately twice the impurity energy. This is consistent with the Lucovsky model (16, 48). The cross section then decays very rapidly in energy, and is essentially zero at 2 eV for Ge and 3.5 eV for Si.

The optical cross sections for transitions to points in the valence band are flat and broad, display very little structure, and are of a relatively small intensity.

As the impurity level is driven closer to the conduction band edge, the cross section maximum is also shifted closer to the conduction band edge. When the impurity level approaches the valence band edge, the optical cross section maximum in the conduction band appears farther from the conduction band edge.

The optical cross sections for deep levels with A1 symmetry associated with anion impurities in GaAs are shown in Figure 4.4. Similar information for GaP and AlP are shown in Figures 4.5 and 4.6. The optical cross section maximum for each of these materials behaves in the same manner as it does for both Si and Ge, that is, as the impurity level is driven closer to the conduction band edge, the optical cross section maximum is closer to the conduction band edge. As the impurity level approaches the valence band edge, the optical cross



section maximum in the conduction band moves farther from the conduction band edge.

The physics of the optical cross sections of deep levels in zincblende and diamond structure semiconductors is very similar when the impurity wavefunctions transform according to A1 symmetry. The cross sections for transitions to the valence bands are broad, flat and of very low intensity while those to the conduction band are very sharp and have their maxima near the conduction band edge. They then decay very rapidly with increasing photon energy and are essentially zero for photon energies greater than about 3 eV.

There are some distinct differences between the cross sections in the two cases, however. For impurities in diamond structure materials, the cross sections for transitions to the conduction band peak at approximately twice the deep level energy. On the other hand, the cross sections for transitions to the conduction bands in zinc-blende semiconductors peak much closer to the conduction band edge. Further, the optical cross sections for impurities in zincblende semiconductors are spread out over a wider range of energies, typically 1 to 2 eV further than those for diamond structure materials. Because of this, as the impurity levels change, there is a more pronounced spreading effect than for diamond semiconductors.

Jaros et al. (17, 78, 85) have predicted optical cross sections for deep level impurities in zincblende and diamond materials. When compared to our theory, their cross sections for transitions to the valence bands are broader (over 5 eV in width) and display several maxima.

As the impurity level is moved closer to the conduction band edge, the maxima shift away from the valence band edge. Some of these peaks may be attributable to differences in the bandstructures used by Jaros and in the present theory. The cross sections for transitions to the conduction bands in both our

theory and Jaros' have a unique peak and behave, at least qualitatively, like those of Lucovsky's model. The closer the impurity level is to the conduction band edge, the closer the maxima are to the band edge in both our theory and that of Jaros.

#### **4.4 Comparison of Direct Gap and Indirect Gap Materials**

As is well-known, direct gap materials are characterized by the lowest conduction band edge occurring at the same  $\vec{k}$ -point of the Brillouin zone as the highest valence band edge. In a direct gap material, optical absorption of a photon occurs by a direct transition at essentially zero wavevector (47, 54, 84). The direct gap semiconductors for which we have chosen to analyze the optical cross sections of deep levels are GaAs and ZnTe.

Indirect gap materials, on the other hand, have their valence band maxima and their conduction band minima occurring at different points in  $\vec{k}$ -space. In order for crystal momentum to be conserved, a photon can only be absorbed with the assistance of a phonon of some (typically large) wavevector (47, 54, 84). The indirect semiconductors which we have selected for analysis are Ge, Si, GaP, and AlP. Although the experimental optical cross sections for these materials clearly includes electron-phonon cooperation, such effects are not included in the present theory, as already mentioned.

##### **4.4.1 Direct Gap Materials**

Optical cross sections for deep levels transforming according to A1 symmetry in GaAs are shown in Figure 4.4. As discussed in the previous section, the cross sections for transitions to the valence bands of GaAs are weak and broad. However, the cross sections for transitions to the conduction bands have maxima very close to the band edge and decay in energy very rapidly. As the impurity level is driven away from the conduction band edge (that is, as the values

change from 1.25 eV to 0.33 eV), the cross section broadens over a wider energy range. The reasons were discussed in detail in the previous section.

When the impurity is located on the cation site and the impurity wavefunction transforms according to T2 symmetry, then the physics changes from the case where it transforms according to A1 symmetry. Such cases are illustrated in Figures 4.7 and 4.8 for the materials GaAs and ZnTe. The jagged peaks which are prevalent in Figure 4.7 for GaAs are due to effects of the bandstructure chosen for our calculations. The cross sections diminish and approach zero when the energy is approximately 5 eV. As the impurity is driven farther from the conduction band edge, the valence band optical cross section remains essentially the same except it does begin to peak closer to the band edge.

In the conduction bands, the cross section maxima rise very sharply near the band edge and then decay very rapidly in energy. As the deep level is driven from the band edge, the optical cross sections do not significantly change their maxima.

For a similar direct gap semiconductor, ZnTe, shown in Figure 4.8, the chemical trends in the optical cross sections for deep levels of T2 symmetry are not very different from those of GaAs (described above) . The very significant difference is that the energy range is larger, simply because the bandwidth is larger.

#### **4.4.2 Indirect Gap Materials**

Optical cross sections for deep levels transforming according to A1 symmetry in GaP are shown in Figure 4.5. Similar to the optical cross sections of other deep levels transforming according to A1 symmetry (discussed in more detail in Section 4.5 which follows), the cross sections for transitions to the valence bands are broad and weak. Cross sections for transitions to the conduction bands are

sharp and strong and reach their maxima in the immediate area of the band edge. As the impurity level is driven further from the band edge, the cross sections broaden and the maxima occur further away from the band edge.

The cross sections for deep levels of A1 symmetry in other indirect semiconductors, such as Si, shown in Figure 4.2, and Ge, shown in Figure 4.3, exhibit similar characteristics. Since the bandgaps and bandwidths of these materials are significantly less than that of GaP, the energy over which the transitions occur is smaller.

Optical cross sections for deep levels transforming according to T2 symmetry in GaP are shown in Figure 4.9. As before, optical cross sections for transitions to both the valence and the conduction bands are sharply peaked and strong in this case. Similar to the optical cross sections of deep levels transforming with A1 symmetry, the cross sections for transitions to the conduction bands reach their maxima very near the band edge and then decay in energy very rapidly. As the impurity level moves farther from the band edge, the maximum shifts slightly closer to the band edge.

The cross section for transitions to the valence band in indirect gap materials have maxima farther from the band edge than similar cross sections in direct gap materials. Also, the energy range is much larger for indirect gap materials than it is for direct gap materials. As the impurity level moves farther from the band edge, the maximum also moves farther from the band edge.

Jaros has also predicted that the intensity of the cross sections is slightly higher for transitions to both the conduction bands and the valence bands in indirect gap materials than for direct gap materials (17, 78, 85). This difference can be attributed to the difference in the bandstructures used in each case.

#### **4.5 Variation in Cross Sections as the Symmetry is Varied**

The optical cross sections for deep levels of A1 symmetry in GaAs with the impurity located at the anion site (refer to Figure 4.4) can be compared to the optical cross sections for deep levels of T2 symmetry in GaAs with the impurity located at the cation site (refer to Figure 4.7). The cross sections for transitions to the conduction bands have very similar characteristics for the two cases. The maxima occur near the conduction band edge and rise very sharply. Nearly all of the cross sections for transitions to the conduction bands occur within a narrow range of energies.

The optical cross sections for transitions to the valence bands where the deep levels transform according to T2 symmetry have several distinct maxima. The first rises very sharply near the valence band edge. All of the cross sections cover a broad range of energies and gradually decline as the energy increases.

The optical cross sections for deep levels of A1 symmetry in GaP with the impurity at the anion site are shown in Figure 4.5. The transitions to the conduction bands are qualitatively similar to those discussed above for GaAs. Also, the comparable optical cross sections for deep levels of A1 symmetry in AIP with the impurity at the anion site (refer to Figure 4.6) possess these same characteristics.

The optical cross sections for deep levels of T2 symmetry for GaP and AIP with the impurity located at the cation site are shown in Figures 4.9 and 4.10, respectively. The trends for these are similar to those associated with those for deep levels of T2 symmetry for GaAs, characterized in the valence bands by a broad range of energies and several maxima.

In the Jaros model, the predicted shapes of the optical cross section for materials with similar symmetries are different from those of our model. In his model, for a transition to the valence band from an A1 symmetric level, there are multiple maxima spread over a broad photon energy range. The cross sections for transitions to the conduction band are of a much lower intensity than our predicted results and rapidly decay in a range of only a few eV. In our theory, we find that the cross section for transitions to the valence bands is small while that for transitions to the conduction bands have a very intense maxima before they, too, decay in intensity.

For a transition to the valence band from a T2 symmetric level, Jaros has predicted cross sections with one maximum and rapidly decaying in energy. For transitions to the conduction band, the cross section intensity in his model is greatly increased and extended over a slightly larger energy range. Our theory predicts optical cross sections of deep level impurities whose wavefunctions transform as T2 symmetry to be very similar to those in Jaros' theory. Also, our theory predicts optical cross sections for A1 symmetric impurities to be similar to Jaros' for transitions to the conduction bands but not for those to the valence bands. Our theory shows flat, broad, low intensity transitions while Jaros predicts broad, jagged, high intensity peaks.

**Figure 4.1. Lucovsky's Model: Optical Cross Section for Deep Level Impurities in Si, Conduction Band Only**

.....  $E_i=1.00$  eV  
-----  $E_i=0.75$  eV  
\_\_\_\_\_  $E_i=0.25$  eV

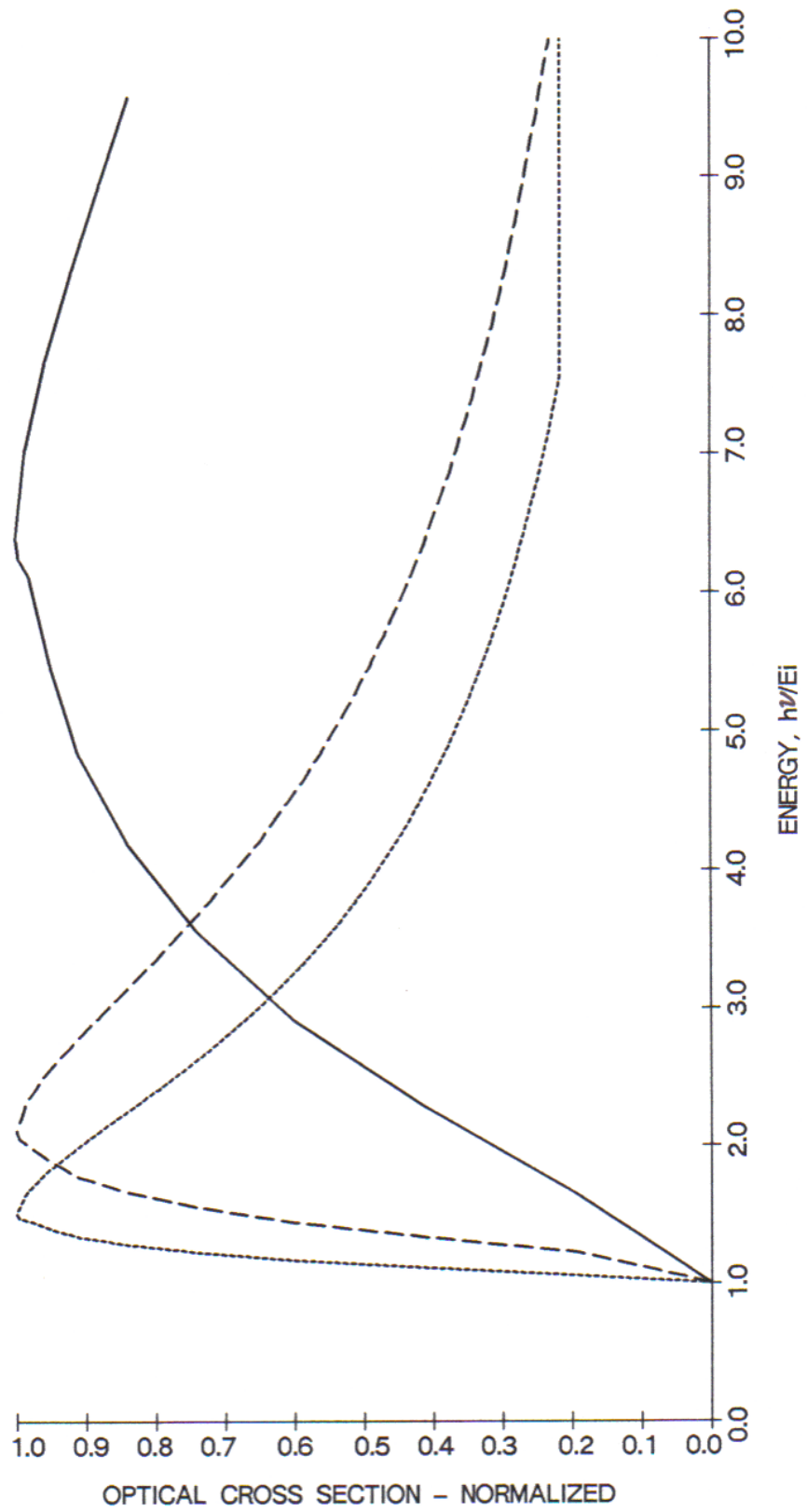




**Figure 4.2. Optical Cross Sections For Deep Levels Of A1 Symmetry In Si With Substitutional Impurities.**

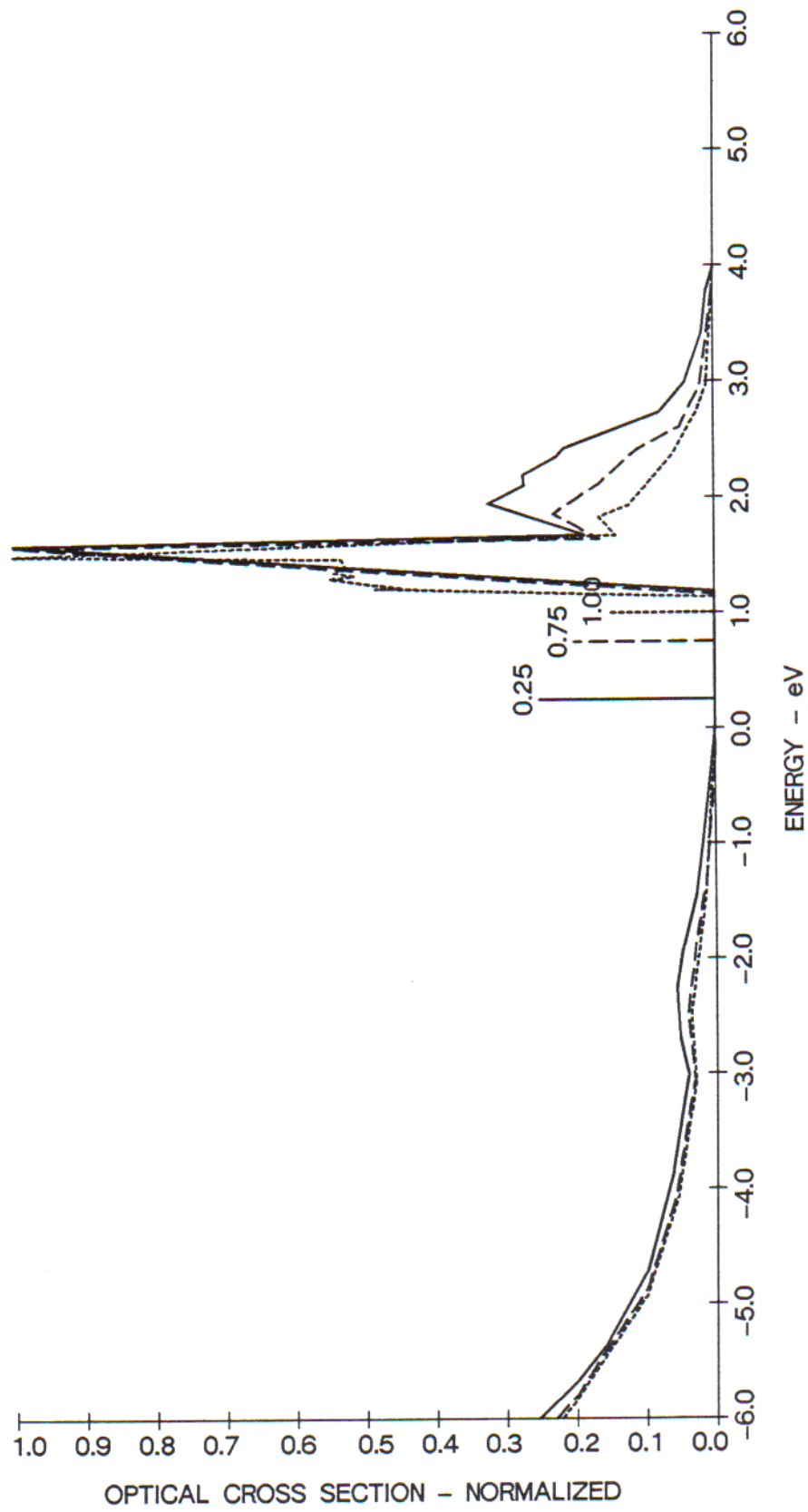


**Figure 4.3. Optical Cross Sections For Deep Levels of A1 Symmetry in Ge With Substitutional Impurities.**

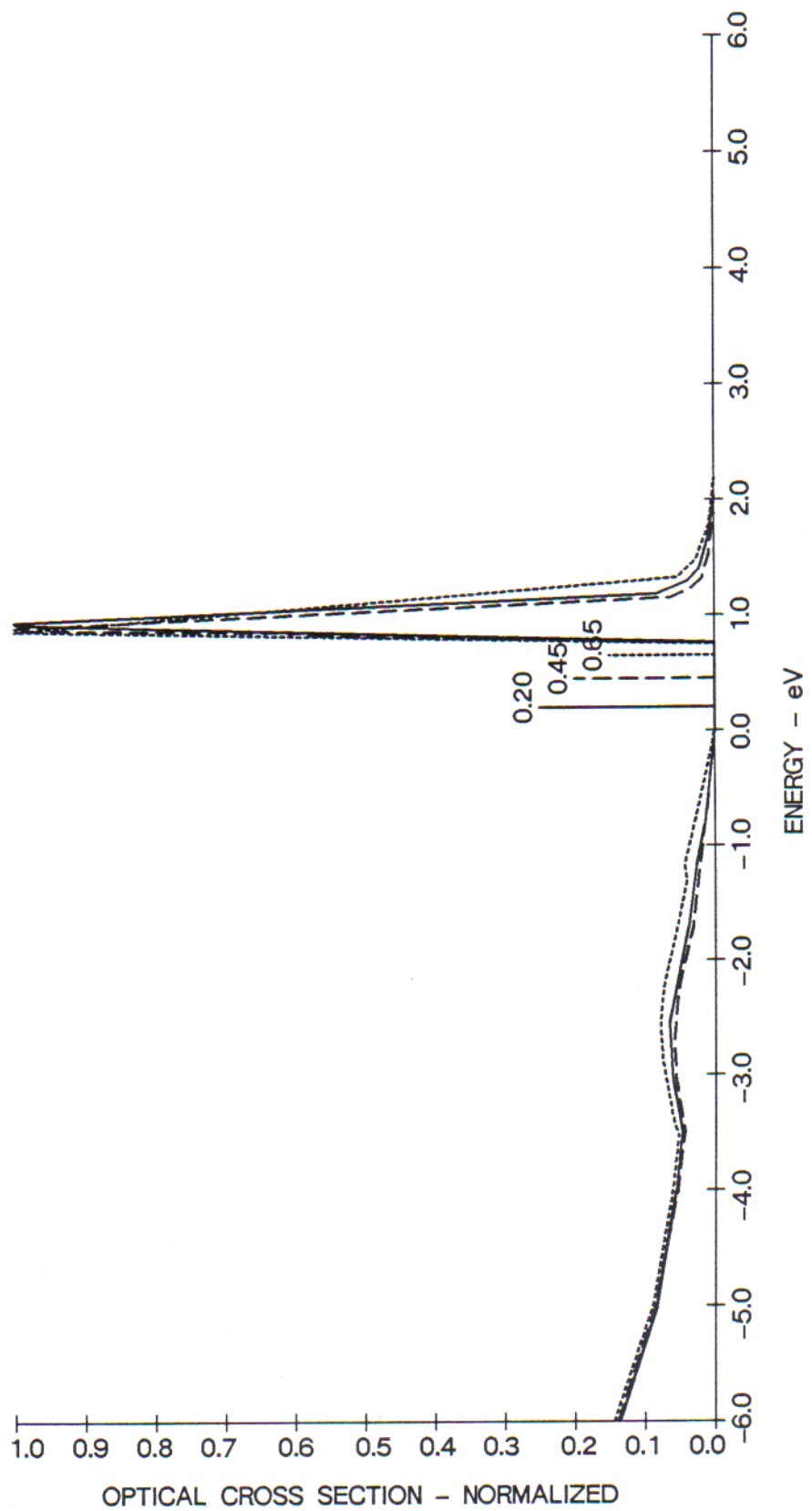


**Figure 4.4. Optical Cross Sections For Deep Levels of A1 Symmetry in GaAs With The Impurity At The As (Anion) Site.**

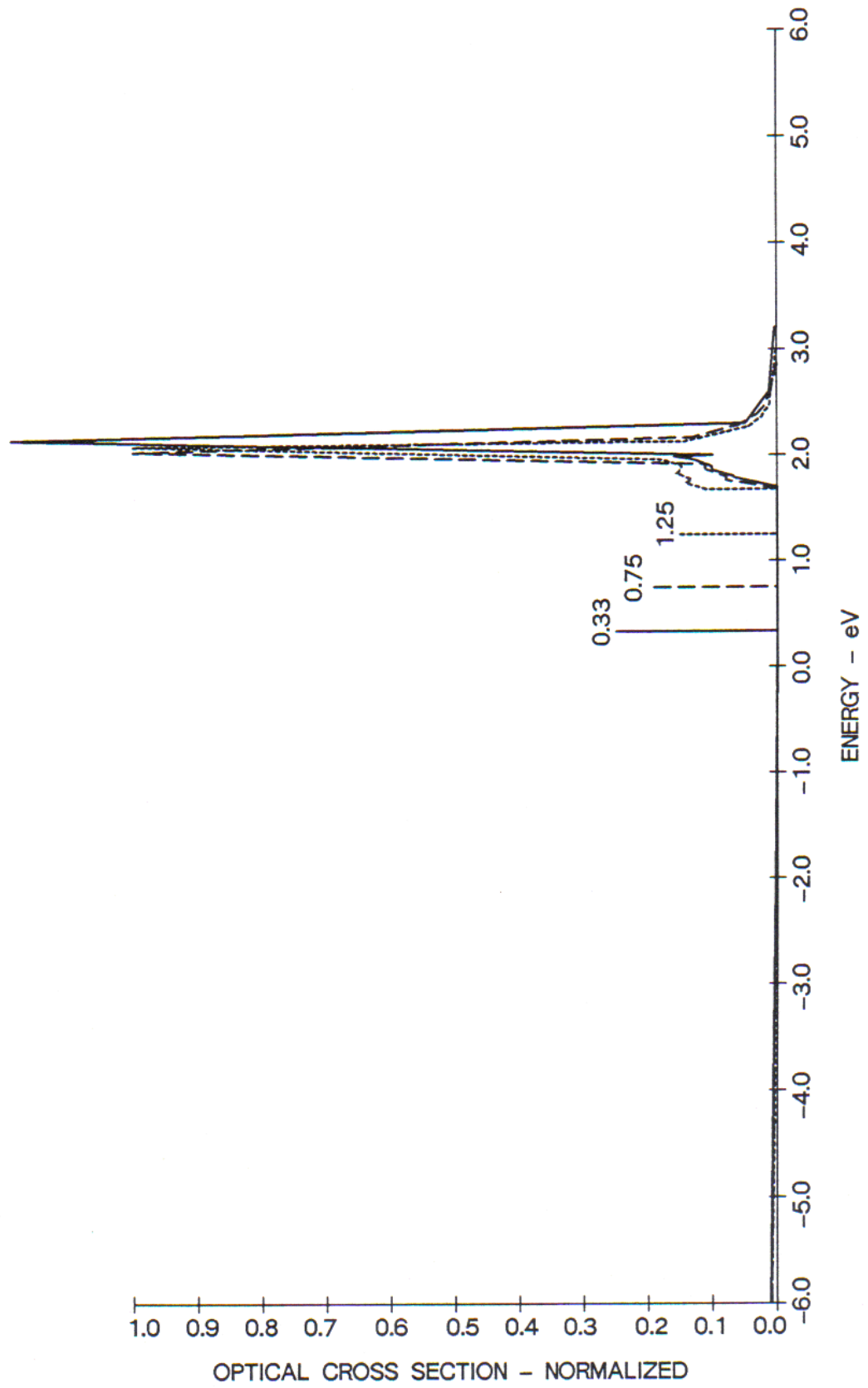


**Figure 4.5. Optical Cross Sections For Deep Levels of A1 Symmetry in GaP With The Impurity At The P (Anion) Site.**

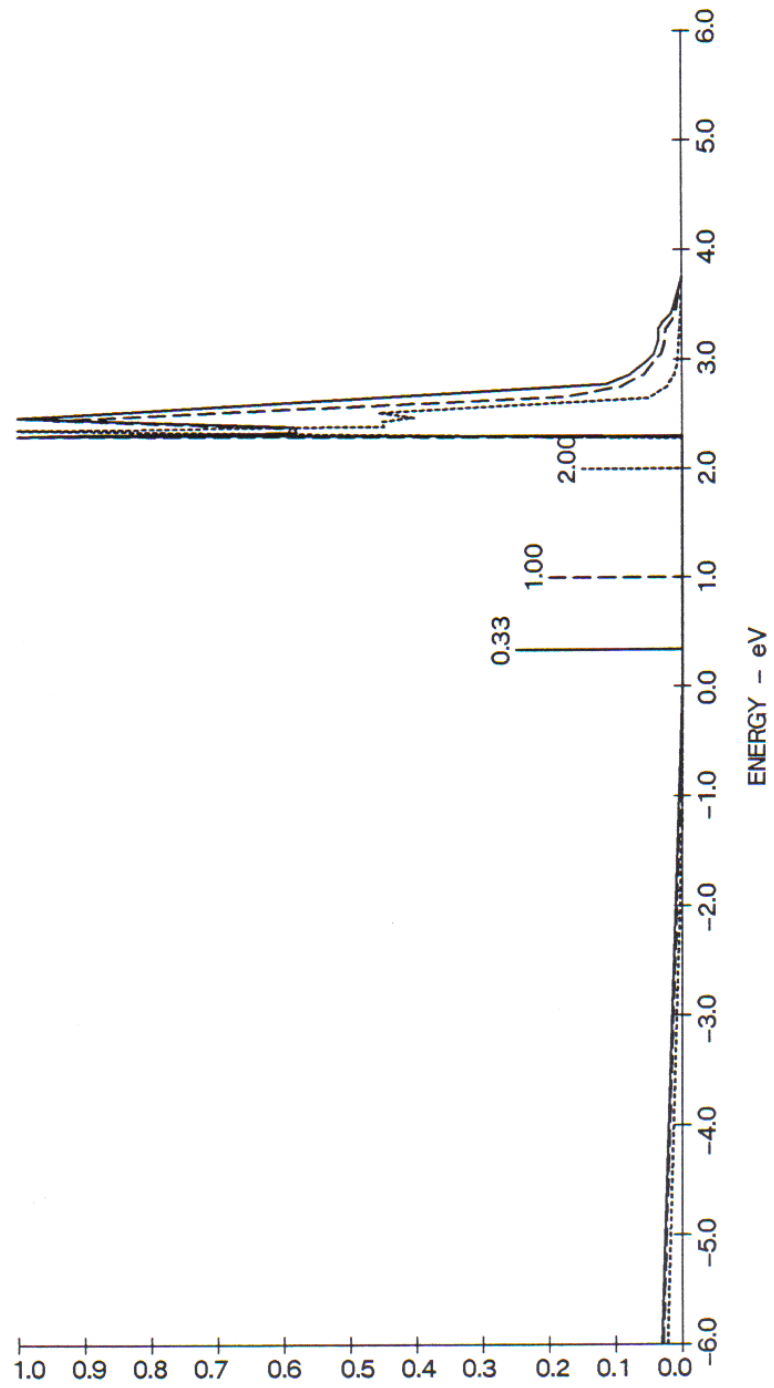




**Figure 4.6. Optical Cross Sections For Deep Levels of A1 Symmetry in AIP With The Impurity At The P (Anion) Site.**

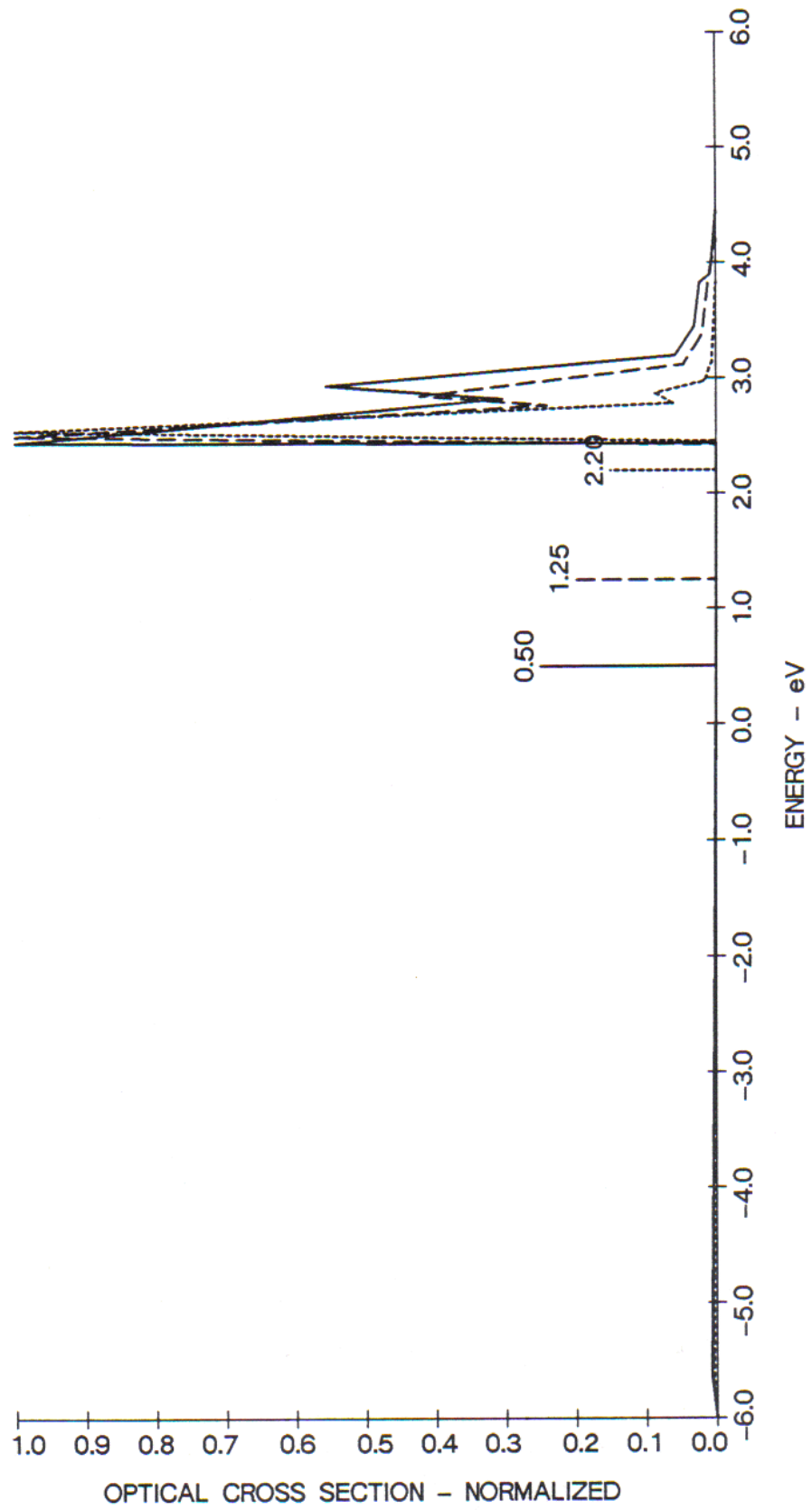


**Figure 4.7. Optical Cross Sections For Deep Levels of T2 Symmetry in GaAs With The Impurity At The Ga (Cation) Site.**

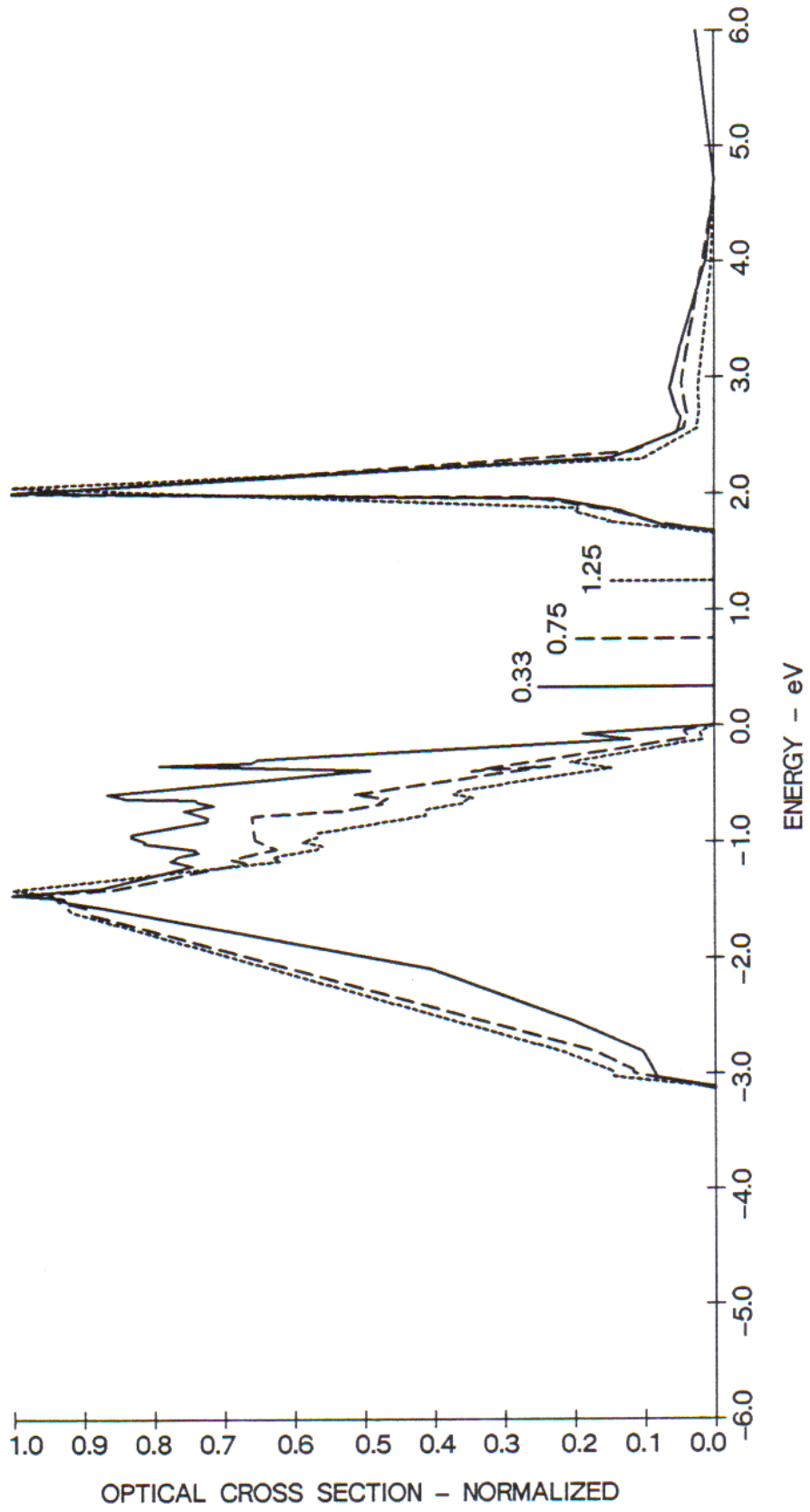


**Figure 4.8. Optical Cross Sections For Deep Levels of T2 Symmetry in ZnTe With The Impurity At The Zn (Cation) Site.**

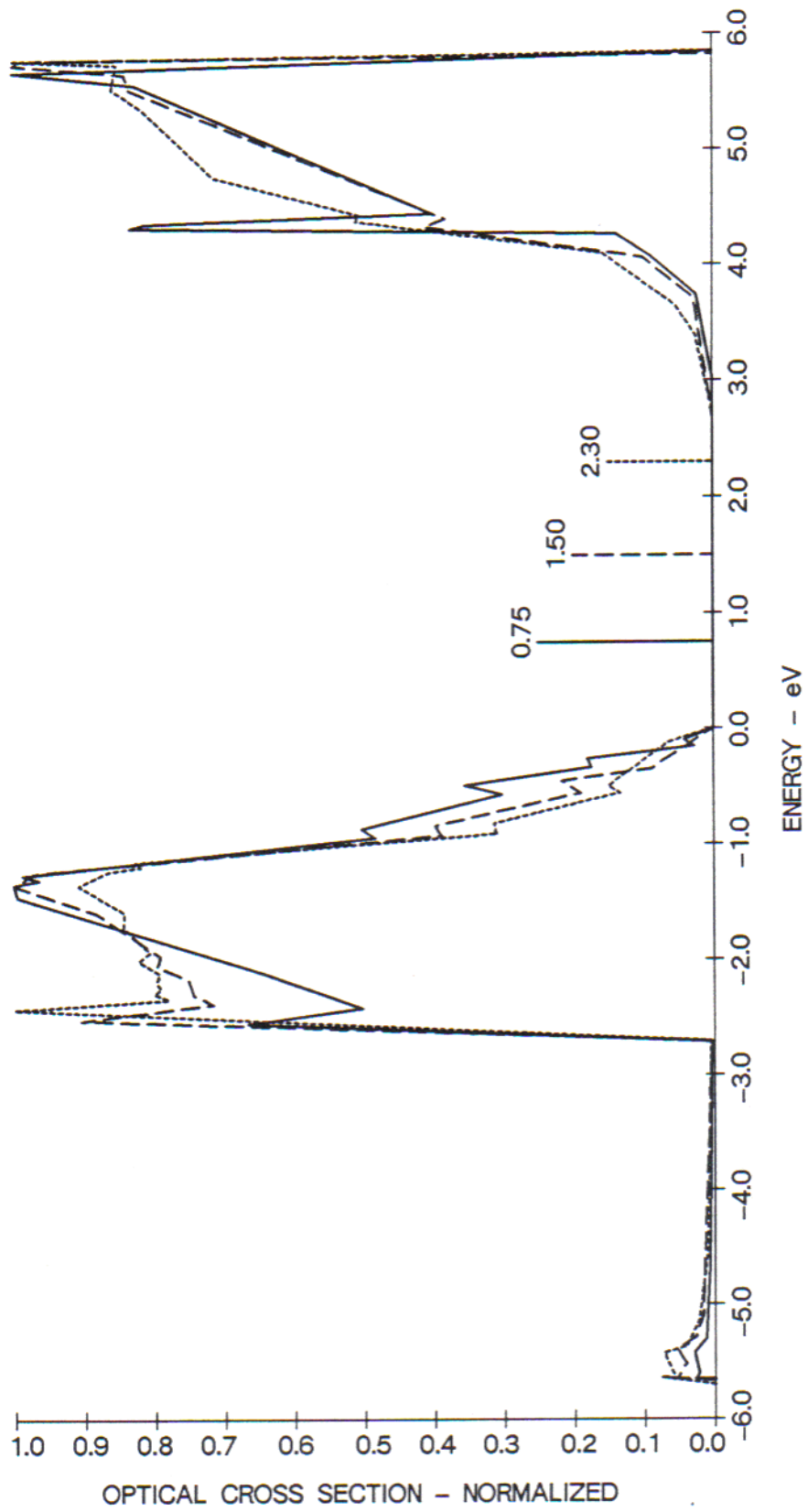


**Figure 4.9. Optical Cross Sections For Deep Levels of T2 Symmetry in GaP With The Impurity At The Ga (Cation) Site.**

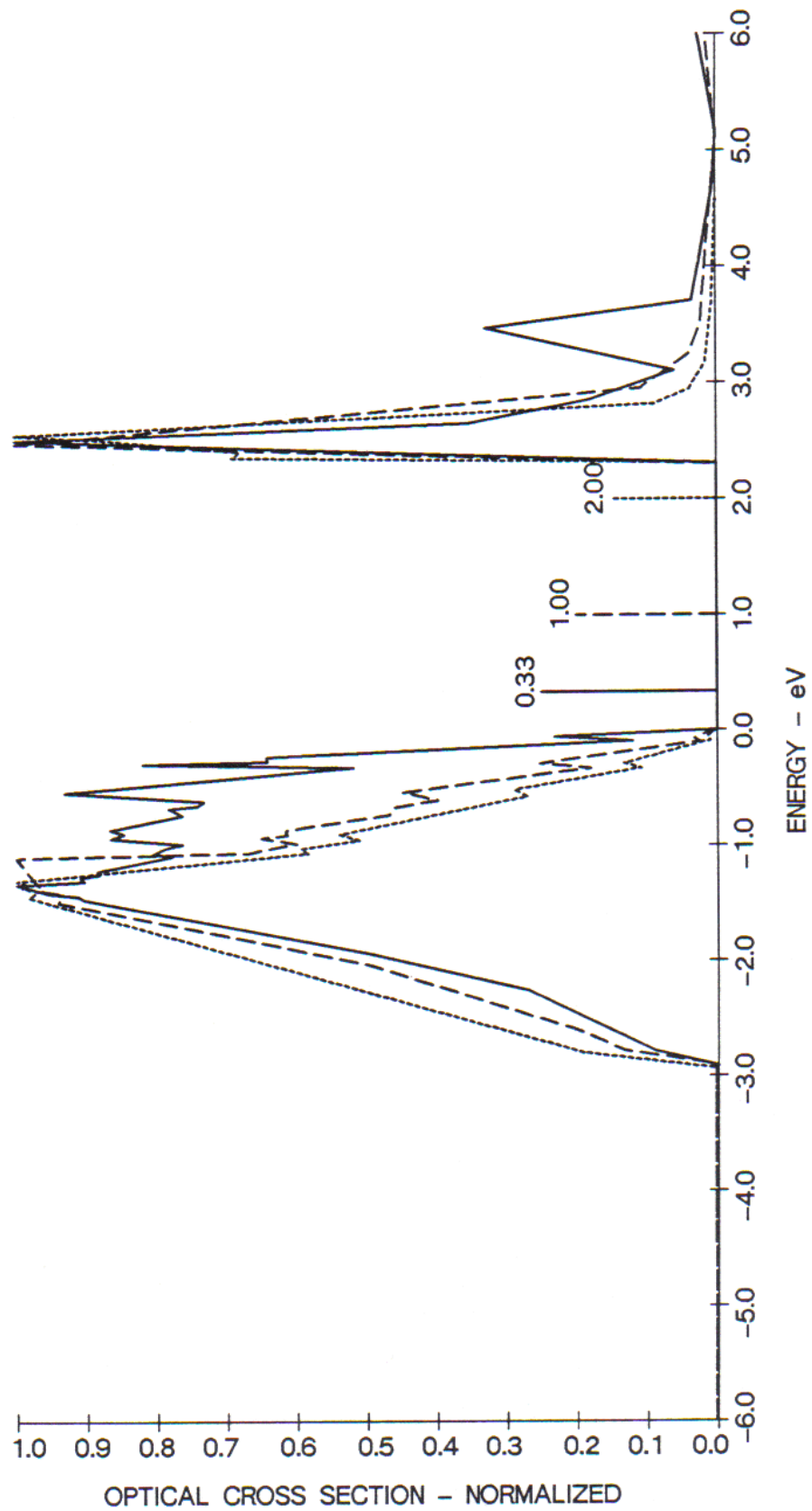
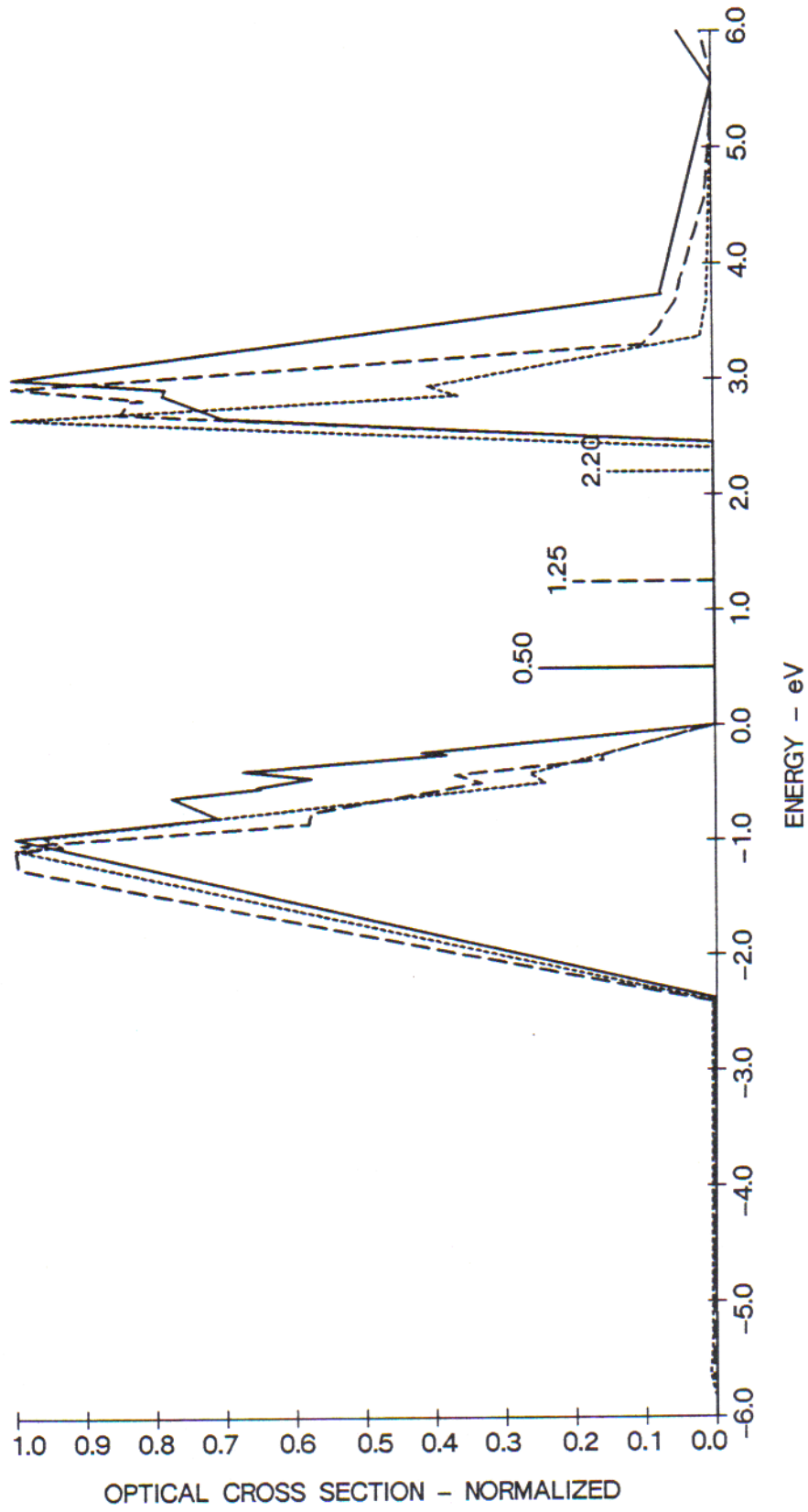




**Figure 4.10. Optical Cross Sections For Deep Levels of T2 symmetry in AIP With The Impurity At The A1 (Cation) Site.**



## CHAPTER V

### CONCLUSIONS

We have developed a model for the calculation of the optical cross section of a deep level impurity in a covalently bonded semiconductor. This formalism is based on quantum mechanical time dependent perturbation theory, assumes a tight binding representation for the host bandstructure, and models the deep level and its associated potential using the Hjalmarson et al. (5, 19) theory of deep levels. Using this formalism, we have numerically calculated the optical cross sections for deep levels of various energies in selected semiconductor hosts. In carrying out these calculations, the Vogl et al. bandstructures were input into the formalism.

In the spirit of the Lucovsky (16) model, and following Hjalmarson, our model assumes a short ranged (central cell) defect only. Also, following the spirit of Hjalmarson's deep level theory, we have assumed that all levels produced by the central cell part of the potential are "deep" regardless of their energy.

While the form of the bandstructures is clearly important for obtaining our numerical results, our formalism is not limited to use with the Vogl et al. theory, and any bandstructure model can be used in the formalism. Different bandstructure models will obviously, however, predict different absolute optical cross sections.

Since the effects of electron-phonon interaction are excluded from our results, the final form of the optical cross section cannot be directly compared or contrasted to experimental results. Our optical cross section curves predict relative intensities and thus can not be used to interpret some details of the cross section. However, the values that we predict for the energies at which the cross section is a maximum should be correct.

We have calculated the optical cross sections for deep levels in selected semiconductors and compared and contrasted these results for deep levels in the zincblende and diamond materials, in direct gap and indirect gap semiconductors, and for impurities whose wavefunctions transform according to the A1 and T2 representations of the Td point group. This allows us to categorize, at least qualitatively, the cross sections of various semiconductor-impurity systems based on these criteria.

## BIBLIOGRAPHY

- (1.) Kassing, R., 1982, Physics of Semiconductor Devices: Proceedings of the International Workshop, November, 1981, New Delhi, India, p551
- (2.) Milnes, A. G., 1973, Deep Impurities in Semiconductors (New York: Wiley-Interscience)
- (3.) Bergh, A. A., and Dean, P. J., 1976, Light Emitting Diodes (Oxford: Clarendon Press)
- (4.) Huang, K. and Rhys, A., 1950, Proc R Soc A 204 406
- (5.) Hjalmarson, H. P., Ph.D. Dissertation, 1979, University of Illinois, Champaign-Urbana
- (6.) Vogl, P., Hjalmarson, H. P., and Dow, J. D., 1983, J Phys C: Solids 5 365
- (7.) Rebane, K. K., 1970, Impurity Spectra of Solids (New York: Plenum Press)
- (8.) Jones, C. E., Nair, V., and Polla, D. L., 1981, Appl Phys Lett 39 248
- (9.) Bebb, H. B., and Chapman, R. A., 1967, J Phys Chem Solids 28 2087
- (10.) Bebb, H. B., 1969, Phys Rev 185 1116
- (11.) Bebb, H. B., and Chapman, R. A., 1971, Proc 3rd photoconductivity Conf, Edited by E. M. Bell (Elmsford: Pergamon Press)
- (12.) Yartsez, V. M., 1974, Phys Stat Solidi 64 377
- (13.) Pantelides, S. T., 1975, Festkorperprobleme XV 149
- (14.) Pantelides, S. T., 1978, Reviews of Modern Physics, Vol 50, No 4, p797
- (15.) Pantelides, S. T. and Harrison, W. A., 1975, Phys Rev B 11 3006
- (16.) Lucovsky, G., 1965, Solid State Commun 3 299
- (17.) Jaros, M., 1982, Deep Levels in Semiconductors (Bristol: Adam Hilger, LTD)

- (18.) Bernholc, J., Lipari, N. O., and Pantelides, S. T., 1978, Phys Rev Lett 41 895
- (19.) Hjalmarson, H. P., Vogl, P., Wolford, D. J., and Dow, J. D., 1980, Phys Rev Lett 44 810
- (20.) Myles, C. W., and Sankey, O. F., 1984, Phys Rev B 29 6810
- (21.) Myles, C. W., Williams, P. F., Chapman, R. A., and Bylander, E. G., 1985, J Appl Phys 57 12
- (22.) Kobayashi, A., Sankey, O. F., and Dow, J. D., 1982, Phys Rev B 25 6367
- (23.) Snyder, P. G., Myles, C. W., Dai, Hong-Hai, and Gundersen, M. A., 1985, Phys Rev B 32 2685
- (24.) Shen, Y. T., and Myles, C. W., 1987, Appl Phys Lett 51 2034
- (25.) Amato, M. A., and Ridley, B. K., 1980, J Phys C: Solid St Phys 13 2027
- (26.) Pena, R. E., and Mattis, D. C., 1981, J Phys C: Solid St Phys 4 647
- (27.) Jaros, M., 1977, Phys Rev B 16 3694
- (28.) Jaros, M., 1980, Advances in Physics, Vol 29, No 3, p409
- (29.) Koster, G. F., and Slater, J. C., 1954, Phys Rev 95 1167; 96 1208
- (30.) Jaros, M., and Brand, S., 1976, Phys Rev B 44 4494
- (31.) Lang, D. V., Logan, R. A., and Jaros, M., 1979, Phys Rev B 19 1015
- (32.) Lin-Chun, P. J., and Reinecke, T. L., 1983, Phys Rev B 27 1101
- (33.) Reinecke, T. L., and Lin-Chun, P. J., 1981, Solid State Commun 40 285
- (34.) DasSarma, S., and Madhukar, A., 1981, Phys Rev B 24 2051
- (35.) Madhukar, A., 1981, Solid State Commun 38 500
- (36.) Tuncay, C., and Tomak, M., 1984, Solid State Commun 50 1065
- (37.) Baraff, G. A., and Schluter, M., 1978, Phys Rev Lett 41 892
- (38.) Jaros, M., and Brand, S., 1979, J Phys C 12 525
- (39.) Lindefelt, U., and Zunger, A., 1982, Phys Rev B 26 846

- (40.) Zunger, A., and Lindefelt, U., 1983, Phys Rev B 27 1191
- (41.) Singh, V. A., and Zunger, A., 1985, Phys Rev B 31 3729
- (42.) Bernholc, J., Lipari, N. O., Pantelides, S. T., and Scheffler, M., 1982, Phys Rev B 26 5702
- (43.) Scheffler, M., Bernholc, J., Lipari, N. O., and Pantelides, S. T., 1984, Phys Rev B 29 3269
- (44.) Sankey, O. F., and Dow, J. D., 1981, Appl Phys Lett 38 685
- (45.) Baraff, G. A., Kane, E. O., and Schluter, M., 1980, Phys Rev B 21 5662
- (46.) Bachelet, G. B., Schluter, M., and Baraff, G. A., 1983, Phys Rev B 27 2545
- (47.) Blow, K. J., and Inkson, J. C., 1980, J Phys C: Solid St Phys 13 539
- (48.) Bernholc, J., and Pantelides, S. T., 1978, Phys Rev B 18 1780
- (49.) Brand, S., 1978, J Phys C: Solid St Phys 11 4963
- (50.) Dow, J. D., Alien, R. E., Sankey, O. F., Buisson, J. P., and Hjalmarson, H. P., 1981, J Vac Sci Technol 19 502
- (51.) Fedders, P. A., and Myles, C. W., 1984, Phys Rev B 29 802
- (52.) Dai, H. H., Gundersen, M. A., and Myles, C. W., 1986, Phys Rev B 33 8234
- (53.) Gregg, J. R., Myles, C. W., and Shen, Y. T., 1987, Phys Rev B 35 2532
- (54.) Kittel, C., 1976, Introduction to Solid State Physics. 5th Edition (New York: John Wiley and Sons, Inc.)
- (55.) Ashcroft, N.W., and Mermin, D. S., 1976, Solid State Physics (New York: Holt, Rinehart, and Winston)
- (56.) Chelikowsky, J. R., and Cohen, M. L., 1976, Phys Rev 14 556
- (57.) Harrison, W. A., 1973, Phys Rev B 8 4487
- (58.) Harrison, W. A., 1975, Phys Rev B 11 3006
- (59.) Harrison, W. A., 1980, Electronic Structure and the Properties of Solids (San Francisco: Freeman Press)

- (60.) Harrison, W. A., and Ciraci, S., 1974, Phys Rev B 10 1516
- (61.) Harrison, W. A., 1977, Festkorperprobleme XVII, p!35
- (62.) Chadi, D. J., and Cohen, M. L., 1975, Phys Stat Solidi 68 405
- (63.) Sankey, O. F., and Dow, J. D., 1981, J Appl Phys 52 5139
- (64.) Sankey, O. F., and Dow, J. D., 1982, Phys Rev B 26 3243
- (65.) Myles, C. W., and Ford, W. C., 1986, J Vac Sci Technol A 4 2195
- (66.) Lee, S., Dow, J. D., and Sankey, O. F., 1985, Phys Rev B 31 3910
- (67.) Ford, W. C., and Myles, C. W., 1986, Phys Rev B 34 927
- (68.) Ho, E. S., and Dow, J. D., 1983, Phys Rev B 27 115
- (69.) Buisson, J. P., Alien, R. E., and Dow, J. D., 1982, Solid State Commun 43 833
- (70.) Myles, C. W., Pen, S. F., Alien, R. E., and Ren, S. Y., 1987, Phys Rev B 35 9758
- (71.) Ford, W. C., Ph.D. dissertation, Texas Tech University, 1986 (unpublished)
- (72.) Monemar, B., and Samuelson, L., 1978, Phys Rev B 18 809
- (73.) Shen, Y. T., 1986, Ph.D. Dissertation, Texas Tech University, Lubbock, Texas
- (74.) Myles, C. W., J Vac Sci Technol, to be published, July, 1988
- (75.) Davydov, A. S., 1976, Quantum Mechanics. 2nd Edition (New York: Pergamon Press)
- (76.) Dexter, D. L., 1958, Solid St Phys 6 355
- (77.) Blakemore, J. S., 1967, Phys Rev 163 809
- (78.) Banks, P.W., and Jaros, M., 1980, J Phys C: Solid St Phys 13 6167
- (79.) Callaway, J., 1964, J Math Phys 5 783
- (80.) Callaway, J., 1964, Electron Band Theory (New York: Academic Press)
- (81.) Ren, S. Y., Hu, W. M., Sankey, O. F., and Dow, J. D., 1982, Physical Review B, Vol 26, No 2, p951



- (82.) Lehman, G., and Taut, M., 1972, Phys Stat Solidi 54, 469 (Fortran program listed in reference 6)
- (83.) Handbook of Chemistry and Physics. 60th Edition. 1979 (Boca Raton, FL: CRC Press, Inc.)
- (84.) Sze, S. M., 1981, Physics of Semiconductor Devices, 2nd Edition (New York: Wiley-Interscience)
- (85.) Jaros, M., and Brand, S., 1976, Physics of Semiconductors (Amsterdam: North Holland)

## APPENDIX A: NUMERICAL ANALYSIS OF THE OPTICAL CROSS SECTION

In order to use the computer program listed in Appendix B, all of the variables must be defined and discussed. The final form of the optical cross section, Eq.(3.40) is

$$\sigma_{1\beta}(h\nu) = (\text{constant} / \hbar) (V_{1\beta}^2 / N) \sum_{n, \vec{k}} \vec{k} \left| \sum \exp(i \vec{k} \cdot \beta \tau_i) \right|^2 |C_{\vec{k}, n, 1\beta}|^2 \times \delta(|E_{1\beta}| + E_{n, \vec{k}} - h\nu) . \quad (\text{A.1})$$

The quantity  $\sum \exp(i \vec{k} \cdot \beta \tau_i)$  must be expanded for the impurity located at the anion site as well as when it is at the cation site.

When the impurity is at the anion site,  $\beta = 0$  and thus

$$\exp(i \vec{k} \cdot \beta \tau_i) = 4 . \quad (\text{A. 2})$$

For the impurity located at the cation site,  $\beta = 1$  and the positions of the four atoms,  $\tau_i$ , must be considered (for zincblende structures, only).

The positions of the four atoms nearest to a central anion are given by

$$\tau_1 = \frac{a}{4} (1,1,1) , \quad (\text{A. 3})$$

$$\tau_2 = \frac{a}{4} (-1,1,-1) , \quad (\text{A.4})$$

$$\tau_3 = \frac{a}{4} (-1,-1,1) , \quad (\text{A.5})$$

and

$$\tau_4 = \frac{a}{4} (1, -1, -1) \quad . \quad (A.6)$$

Thus we have

$$\vec{K} \tau_1 = \frac{a}{4} (kx + ky + kz) \quad , \quad (A.7)$$

$$\vec{K} \tau_2 = \frac{a}{4} (-kx + ky - kz) \quad , \quad (A.8)$$

$$\vec{K} \tau_3 = \frac{a}{4} (-kx -ky + kz) \quad , \quad (A.9)$$

and

$$\vec{K} \tau_4 = \frac{a}{4} (kx -ky -kz) \quad , \quad (A.10)$$

where  $a$  is the lattice constant.

Expanding the exponential function, we have

$$\begin{aligned} \left| \sum_i \exp i \vec{K} \cdot \tau_i \right|^2 = & \exp \left[ \left( \frac{ia}{4} \right) (kx +ky +kz) \right] \\ & + \exp \left[ \left( \frac{ia}{4} \right) (-kx +ky -kz) \right] \\ & + \exp \left[ \left( \frac{ia}{4} \right) (-kx -ky +kz) \right] \\ & + \exp \left[ \left( \frac{ia}{4} \right) (kx -ky -kz) \right] \quad . \quad (A.11) \end{aligned}$$

Combining terms and using the trigonometric identity,

$$\cos (A \pm B) = \cos A \cos B \mp \sin A \sin B \quad , \quad (A.12)$$

one obtains,

$$\begin{aligned}
\left| \sum_i \exp i \vec{k} \cdot \tau_i \right|^2 = & 4 \left[ 1 + \cos \left( kx \frac{a}{2} \right) \cos \left( ky \frac{a}{2} \right) \right. \\
& + \cos \left( kx \frac{a}{2} \right) \cos \left( kz \frac{a}{2} \right) \\
& \left. + \cos \left( ky \frac{a}{2} \right) \cos \left( kz \frac{a}{2} \right) \right]. \tag{A.13}
\end{aligned}$$

For  $\beta = 0$ , the equation simplifies to

$$\left| \sum_i \exp i \vec{k} \cdot \tau_i \right|^2 = 16 \tag{A.14}$$

A numerical technique for calculating generalized state densities was used to numerically evaluate the optical cross section. This technique was originally developed by Lehman and Taut (82) and later modified by Hjalmanson (5). This technique calculates a generalized density of states function of the following form:

$$D(E) = \frac{1}{N} \sum_{\vec{k}, n} F_n(\vec{k}) \delta(E - E_n, \vec{k}) \tag{A.15}$$

It can easily be shown that the optical cross section, Eq. (3.40) has this form with  $E = |E_i| - h\nu$  and

$$F_n(\vec{k}) = \vec{k}^2 \left| \sum_i \exp i \vec{k} \cdot \tau_i \right|^2 C(\vec{k})^2_{n,i\beta} \tag{A.16}$$

and

$$\vec{k}^2 = (kx)^2 + (ky)^2 + (kz)^2 \tag{A.17}$$

Each of the variables comprising the optical cross section equation Eq. (3.40) are shown below with its

variable name as it appears in the computer model listing in Appendix B.

$$\left| \sum_i \exp i \vec{k} \cdot \tau_i \right|^2 = \text{EX(L,ICNT)} \quad (\text{A.18})$$

$$\vec{k}^2 = \text{RK(ICNT)} \quad (\text{A.19})$$

$C(\vec{k})_{n,i\beta}$ :

$$C(1,\text{NBAND}) = G0(1,\text{NBAND}) \text{ for A1 , anion} \quad (\text{A.20})$$

$$C(2,\text{NBAND}) = G0(2,\text{NBAND}) \text{ for T2 , anion} \quad (\text{A.21})$$

$$C(3,\text{NBAND}) = G0(1,\text{NBAND}) \text{ for A1, cation} \quad (\text{A.22})$$

$$C(4,\text{NBAND}) = G0(2,\text{NBAND}) \text{ for T2 , cation} \quad (\text{A.23})$$

$$E_i = E_L \quad (\text{A.24})$$

$$V_{1\beta} = 1 (E^{\text{impurity}} - E^{\text{host}}) \quad (\text{A.25})$$

$$1 = 0.6 \text{ for T2 symmetry} \quad (\text{A.26})$$

$$1 = 0.8 \text{ for A1 symmetry} \quad (\text{A.27})$$

$$E_n(\vec{k}) = E(\text{NBAND,ICNT}) \quad (\text{A.28})$$

$$h\nu - |E_{1\beta}| = X(1) \quad (\text{A.29})$$

$$h\nu = E_1 - E \text{ for the valence band} \quad (\text{A.30})$$

$$h\nu = E - E_1 \text{ for the conduction band} \quad (\text{A.31})$$

$$h\nu = |E - E_1| \geq 0 \quad (\text{A.32})$$

$$= |X(1) + E_L| \quad (\text{A.33})$$

where  $X(1)$  is the energy with respect to the top of valence band.

**APPENDIX B: OPTICAL CROSS  
SECTION PROGRAM LISTING**

```
C PROGRAM TO DO OPTICAL CROSS SECTIONS FOR COVALENTLY
C BONDED SEMICONDUCTORS. C IMPLICIT REAL*8(A-H,O-Z)
C THIS WAS WRITTEN BY L. RICKS HAUENSTEIN, COMPLETED
C JANUARY, 1988
C SET UP TO USE NEAREST NEIGHBOR SP3S* BANDSTRUCTURES
C FOR ZINCBLLENDE AND DIAMOND LATTICE MATERIALS
  LOGICAL ITRUE,IFLS
  DIMENSION OCSR(1060),OCSI(1060),X(1060),EN(10),C(4)
  DIMENSION DENSYM(13),PARAM(13),E1(14),E2(14)
  DIMENSION EX(2,530), DER(1060,10),DEI(1060,10)
  DIMENSION DENSR(1060),DENSI(1060),XU(1060)
  DIMENSION RK(286),G0(2,10),61(2,10),601(4,4,10)
  COMMON/EANDA/E(10,286),AR(10,286),AI(10,286)
  COMMON/AKTEST/ITRUE,IFLS
  COMMON/LATSYM/IPLANE
  COMMON/PARAMS/PARAM
  DATA NN,ID1,BL,BETA/0,5,0.8,0./
  DATA KPTS,MPTS,MXC,MXIJC,NPTS/186,1060,1,1,1060/
  DATA F0,VALGAM/0.E+0,0.E+0/
  DATA NKGAMX,NBAND,NINCR,EI,EF,NPTS/10,1,1,-13.,-13./
  DATA IITRU/1/
  DATA INDEX/0/
  DATA ZERO,ONE,TWO,THREE,FOUR/0.,1.,2.,3.,4./
  DATA PI/3.141592654/
  IF(BETA.EQ.0.)GO TO 60
  IF(BL.EQ.0.8)GO TO 80
  IF(BL.EQ.0.6)GO TO 95
60  IF(BL.EQ.0.8)GO TO 70
```

```

IF(BL.EQ.0.6)GO TO 90
70      K = 1
        L=1
        GO TO 1000
80      K = 3
        L=2
        GO TO 1000
90      K = 2
        L=1
        GO TO 1000
95      K = 4
        L = 2
1000  CONTINUE
      IF(BL.EQ.0 .8)GO TO 96
      VL=0.6*(EM-EH)
      GO TO 97
96     VL=0.8*(EM-EH)
97     CONTINUE
C
C
      IPLANE=1000
      NBM=10
C     INDEX=0;FCC;;;INDEX=1;SC.
C     IITRU=0,DOS;;IITRU=1,GENERALIZED DOS.
      WRITE(6,1) C
      RNPTS=NPTS
      EGRID=(EF-EI)/RNPTS
      WRITE(6,901)NKGAMX,NBAND,NINCR,IITRU,EI,EF,EGRID
C
      ITRUE=.FALSE.
      IFLS=.TRUE.

```

```

        IF(IITRU.GT..5)ITRUE=.TRUE.
        IF(IITRU.GT..5)IFLS=.FALSE.
        IF(TRUE)MXC = 4
C IF FCC SET IPLANE WITH NEXT LINE
        IF(INDEX.EQ.0)IPLANE=3*(NKGAMX/2)
        IF(NPTS.LE.MPTS)GO TO 2
        WRITE(6,905)NPTS,MPTS
        CALL EXIT
        WRITE(6,902)NPTS
        DO 230 I=1,NPTS
        X(I)=(FLOAT(I-1)*EGRID+EI)
        XU(I)=ABS(X(I)-EL)
230 CONTINUE
        N1=NKGAMX+1
        XN1=FLOAT(NKGAMX)
        KMAX=(NI*(NI+1)*(NI+2))/6
        WRITE(6,903)KMAX,KPTS
        IF(KMAX.GT.KPTS)CALL EXIT
        IF(BETA.EQ.1.)GO TO 55
        DO 54 10=1,101
        INDX=(ID-1)*13
C READ TIGHT BINDING PARAMETERS
        READ(24,540)(DENSYM(INDX+II),11=1,9)
        READ(24,510)(DENSYM(INDX+II),11=10,13)
54 CONTINUE GO TO 58
55 DO 58 ID=1,ID1
        INDX=(ID-1)*13
        READ(25,540)(DENSYM(INDX+II),11=1,9)
        READ(25,510)(DENSYM(INDX+II),11=10,13)
58 CONTINUE
        DO 59 11=1,13

```



```

INDX=(ID1-1)*13
PARAM(II)=DENSYM(INDX+II)
59  CONTINUE
DO 10 IIX=1,N1
DO 10 IIY=1,IIX
DO 10 IIZ=1,IIY
IF(IIX+IIY+IIZ-3.GT.IPLANE)GO TO 10
XK=FLOAT(IIX-1)/XN1
YX=FLOAT(IIY-1)/XN1
ZX=FLOAT(IIZ-1)/XN1
XX=PI*XK
YY=PI*YK
ZZ=PI*ZK
ICNT=((IIX**2-1)*IIX)/6+((IIY-1)*IIY)/2+IIZ
INCT0=ICNT
EX(1,ICNT)=16.
EX(2,ICNT)=4.+(2.*COS(XX+ZZ))+2.*COS(XX+YY) )
1+{2 .*COS (YY+ZZ) )+(2 .*COS (YY-ZZ) )
2+(2.*COS(XX-YY))+2.*COS(XX-ZZ))
C CALL PAIRSM TO COMPUTE EIGENVALUES AND EIGENVECTORS
C USED TO CALCULATE THE HOST GREEN'S FUNCTION. ENERGIES
C ARE DEVELOPED FOR THE 10 BAND TIGHT BINDING MODEL. ALL
C CALCULATIONS ARE PERFORMED ASSUMING NN=0, THAT IS, FOR
C A SINGLE DEFECT.
CALL PAIRSM(XK,YK,ZK,EN,NN,G01,G0,G1)
IF(ICNTO.EQ.I)VALGAM=EN(4)
DO 2000 NBAND=1,NBM
C(1,NBAND)=G0(1,NBAND)
C(2,NBAND)=G0(2,NBAND)
C(3,NBAND)=G0(1,NBAND)
C(4,NBAND)=G0(2,NBAND)

```

```

E(NBAND,ICNT)=EN(NBAND)-VALGAM
IF(IFLS)GO TO 10
MXIJC=MXC
RK(ICNT) =(XK**2.)+(YK**2.) +(ZK**2.)
AR(NBAND,ICNT)=RK(ICNT)*(C(K,NBAND)**2.)*(EX(L,ICNT))
AI(NBAND,ICNT)=ZERO
6   CONTINUE
2000 CONTINUE
10  CONTINUE
WRITE(6,340)VALGAM
IJC = 1
DO 350 I=1,NPTS
DENSР(I)=F0
DENSI(I)=F0
OCSR(I)=F0
OCSI(I)=F0
350 CONTINUE
IDUM=IJC
C SUBROUTINE DENSE5 COMPUTES THE GENERALIZED DOS.
CALL DENSE5(DER,DEI,EI,EF,EGRID,NKGAMX,NPTS,
11,NBM,NINCR,IDUM)
DO 360 NBAND=1,NBM,NINCR
DO 360 I=1,NPTS
DENSР(I)=DENSР(I)+DER(I,NBAND)
DENSI(I)=DENSI(I)+DEI(I,NBAND)
360 CONTINUE
RNBM=NBM
FMAXP=0.
FMAXN=0.
DO 361 I=1,NPTS
C CALCULATE THE OPTICAL CROSS SECTION

```

```

OCSR(I)=(DENSR(I)/RNBM)*((VL/(2*EL-XU(I)))**2/XU(I)
OCSI (I) = (DENSI (D/RNBM) * ( VL/ ( 2*EL-XU (I) ) ) **2/XU(I)
C NORMALIZE BOTH HALVES OF THE CURVE
IF(X(I) .LT.0.)GO TO 351
IF(OCSR(I).GT.FMAXN)FMAXN=OCSR(I)
GO TO 361
351 IF(OCSR(I).GT.FMAXP)FMAXP=OCSR(I)
361 CONTINUE
DO 352 I=1,NPTS
IF(X(I) .LT.0.)GO TO 353
OCSR(I)=OCSR(I)FMAXN
GO TO 352
353 OCSR(I)=OCSR(I)FMAXP
352 CONTINUE
PRINT 951,IJC
PRINT 952
PRINT 950,(X(I) ,DENSR(I) ,DENS(I) ,I=1,NPTS)
WRITE(12,931) (X(I) ,OCSR(I) ,I=1,NPTS)
300 CONTINUE
310 CONTINUE
1 FORMAT(IX,'WRITTEN BY L. R. HAUENSTEIN, LAST MODIFIED
1ON APRIL 8, 1987. ')
340 FORMAT(IX,'ZERO OF ENERGY AT1,EII.4)
500 FORMAT(10F8.4)
505 FORMAT(2E10.2)
510 FORMAT(4F8.4)
520 FORMAT(5F8.2)
530 FORMAT(1F8.2)
540 FORMAT(9F8.4)
902 FORMAT(IX,'NPTS',14)
903 FORMAT(IX,'NUMBER OF POINTS IN SC IRRED WEDGE',15,

```

```
1/,1X,'MUST BE LESS THAN',15)
905  FORMAT(' ', 'NPTS= ',15,' .GT. MPTS = ',15)
931  FORMAT(2F15.4)
950  FORMAT(2X,3E16.7)
951  FORMAT(////2X,'TOTAL DOS FOR IJC=',I4)
952  FORMAT(2X,'E ',10X,'DOSR',15X,'DOSI)
STOP
END
```